JACS
JOURNAL OF THE AMERICAN CHEMICAL SOCIETY
Article
pubs.acs.org/JACS

Diagnostic Imaging Agents for Alzheimer's Disease: Copper Radiopharmaceuticals that Target Aβ Plaques

James L. Hickey,[†,‡] SinChun Lim,[†,‡] David J. Hayne,[†,‡] Brett M. Paterson,[†,‡] Jonathan M. White,[†,‡] Victor L. Villemagne,[§,∞] Peter Roselt,[⊥] David Binns,[⊥] Carleen Cullinane,[∥,⊥] Charmaine M. Jeffery,[#] Roger I. Price,[#,¶] Kevin J. Barnham,[‡,□,§] and Paul S. Donnelly*[,†,‡]

[†]School of Chemistry, [‡]Bio21 Molecular Science and Biotechnology Institute, [§]Florey Institute of Neuroscience and Mental Health, [□]Department of Pharmacology, and [∥]Department of Pathology, University of Melbourne, Parkville, Melbourne, Victoria, 3010, Australia

[⊥]The Molecular Imaging and Targeted Therapeutics Laboratory, Peter MacCallum Cancer Centre, St Andrews Place, East Melbourne, Victoria, Australia

[∞]Centre for PET, Austin Hospital, Heidelberg, Victoria 3084, Australia

[#]Department of Medical Technology and Physics, Sir Charles Gairdner Hospital, Nedlands, Western Australia, Australia

[¶]School of Physics, The University of Western Australia, Nedlands, Western Australia, Australia

Supporting Information

ABSTRACT: One of the pathological hallmarks of Alzheimer's disease is the presence of amyloid-β plaques in the brain and the major constituent of these plaques is aggregated amyloid-β peptide. New thiosemicarbazone-pyridylhydrazine based ligands that incorporate functional groups designed to bind amyloid-β plaques have been synthesized. The new ligands form stable four coordinate complexes with a positron-emitting radioactive isotope of copper, ^{64}Cu. Two of the new Cu^{II} complexes include a functionalized styrylpyridine group and these complexes bind to amyloid-β plaques in samples of post-mortem human brain tissue. Strategies to increase brain uptake by functional group manipulation have led to a ^{64}Cu complex that effectively crosses the blood-brain barrier in wild-type mice. The new complexes described in this manuscript provide insight into strategies to deliver metal complexes to amyloid-β plaques.

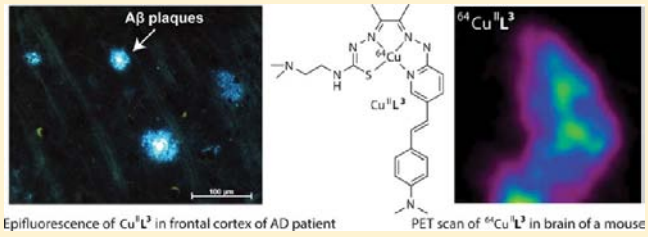

Epifluorescence of $Cu^{II}L^3$ in frontal cortex of AD patient
PET scan of $^{64}Cu^{II}L^3$ in brain of a mouse

INTRODUCTION

Alzheimer's disease (AD) is the major cause of dementia and is a progressive neurodegenerative disorder that leads to synaptic failure and neuronal death. The disease is characterized by a gradual onset and progression of cognitive deficits in several domains including episodic memory, attention, and language.[1] One of the major pathological hallmarks of the disease is the presence of extracellular senile plaques in the brain. The major constituent of these plaques is an insoluble aggregated peptide called amyloid-β (Aβ), a 39−43 amino acid peptide derived from the amyloid precursor protein (APP).[2,3] Although the exact role of Aβ plaques in the onset of dementia remains controversial, what is certain is that histopathological studies show extensive cortical Aβ deposition in post-mortem analysis of AD subjects.[4] At present, clinical diagnosis of AD is based on tests to establish progressive impairment of memory and at least one other area of cognition. Definite diagnosis of AD relies on the presence of plaques and neurofibrillary tangles identified by post-mortem analysis.[1,5]

Aβ fibrils adopt a cross-β-sheet structure with highly ordered monomers aggregated by virtue of hydrogen bonding, π−π stacking of aromatic residues and electrostatic interactions (glutamate − lysine). Aβ1−42 contains hydrophobic segments both in the middle (residues 17−21) and at the C terminus (residues 30−40). The parallel orientation of β sheet structures generates small channels and hydrophobic pockets that extend along the length of the filament to which aromatic molecules can intercalate and bind by way of π−π interactions.[4,6] A range of benzothiazole and stilbene compounds bind with some degree of selectivity to Aβ fibrils and plaques.[4] The chemical structure of stilbenes and benzothiazoles display some similarities. They both contain highly conjugated rigid aromatic ring systems, and derivatives with electron-donating groups at each end of the molecule display the highest affinity for Aβ fibrils. It is thought that these molecules enter a hydrophobic pocket or channel and bind by way of a combination of hydrophobic and π−π interactions. It is likely that there is more than one such binding site on the presumed β-sheet aggregates present in Aβ plaques.[4]

Diagnostic imaging using positron emission tomography (PET) is a powerful technique to study the molecular nature of

Received: June 9, 2013
Published: September 26, 2013

   dx.doi.org/10.1021/ja4057807 | J. Am. Chem. Soc. 2013, 135, 16120−16132

disease in living patients. PET imaging of Aβ plaque burden is possible using radiolabeled benzothiazole or stilbene derivatives that are capable of crossing the blood-brain barrier and binding selectively to Aβ plaques.[7−9] A benzothiazole derivative radiolabeled with the positron-emitting radioactive isotope carbon-11, ^{11}C-PIB (Pittsburgh compound B) (Figure 1), has

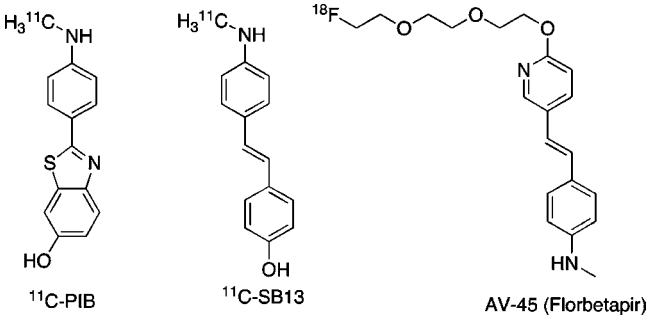

Figure 1. Benzothiazole, stilbene and styrylpyridine Aβ targeting radiolabeled compounds ^{11}C-PIB, ^{11}C-SB13, and ^{18}F-AV45.

proven useful in characterizing plaque burden in humans and early diagnosis AD pathology by PET imaging.[7,8,10−12] A stilbene derivative radiolabeled with carbon-11 (4-*N*-methyl-amino-4′-hydroxystilbene), known as SB-13,[9] binds selectively to Aβ plaques (Figure 1).[13] Preliminary studies of SB-13 in humans were promising and stimulated continued explorations of stilbene and styrylpyridine derivatives as probes for the detection of Aβ plaques.[4,14] A stilbene derivative proved to have some selectivity for amyloid plaques over other aggregates such as neurofibrillary tangles and Lewy bodies and as such has the potential to be of use in the differential diagnosis of AD from other conditions.[15]

The longer half-life of fluorine-18 when compared to carbon-11 has several advantages and fluorine-18 has become the most widely used radionuclide for PET imaging. Recent efforts focusing on preparing stilbene[16] or styrylpyridine[17,18] derivatives radiolabeled with fluorine-18 have culminated with the recent FDA approval of ^{18}F-AV45 (florbetapir) (Figure 1) to detect the presence of amyloid.[4,5,19−21]

Both fluorine-18 and carbon-11 must be attached covalently, to plaque binding molecules, and this can lead to complicated synthetic manipulations requiring specialist equipment. In addition, both isotopes are handicapped by a relatively short half-life (^{11}C = 20.4 min, ^{18}F = 109.7 min). In principle, the rapid and simple incorporation of a radioactive metallic isotope into a specific targeting ligand is an attractive alternative. Copper in particular has several positron-emitting isotopes, with half-lives ranging from 9.7 min for ^{60}Cu to 12.7 h for ^{64}Cu.[22−26] A bis(thiosemicarbazone) ligand radiolabeled with copper radioactive isotopes, Cu^{II}(atsm) (Figure 2), is currently being assessed in clinical trials as a hypoxia imaging agent in head and neck cancer.[27,28] Our initial attempts at designing a copper radiopharmaceutical suitable for plaque imaging resulted in a Cu^{II}(atsm) derivative with an appended stilbene functional group linked to the ligand framework *via* a thiocarbohydrazone linkage.[29] This Cu^{II}(atsm) derivative was relatively difficult to radiolabel with Cu-64 and best radiolabeling was achieved *via* a transmetalation reaction of a Zn^{II} complex.[29,30] In addition, the thiocarbohydrazone linkage could be susceptible to hydrolysis. Hybrid thiosemicarbazonato-pyridylhydrazide ligands form charge neutral Cu^{II} complexes

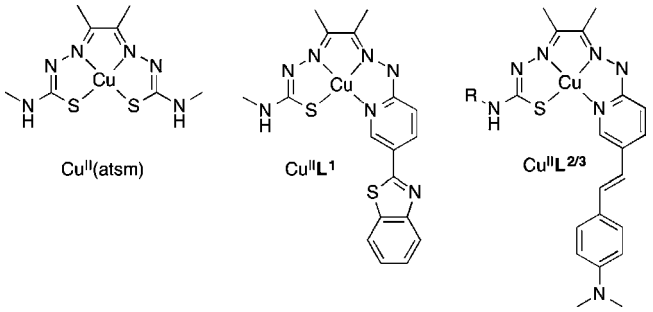

Figure 2. Structures of bis(thiosemicarbazonato)Cu^{II} complexes Cu^{II}(atsm) and new hybrid thiosemicarbazonato-pyridylhydrazide Cu^{II} complexes with Aβ plaque targeting benzothiazole ($Cu^{II}\mathbf{L}^1$) and styrylpyridine functional groups ($Cu^{II}\mathbf{L}^2$ R = CH_3; $Cu^{II}\mathbf{L}^3$ R = $CH_2CH_2N(CH_3)_2$).

with a Cu^{II}/Cu^{I} reduction potential 100 mV more negative than Cu^{II}(atsm). Preliminary studies identified copper complexes of these hybrid ligand systems as being more stable than Cu^{II}(atsm) suggesting that Cu^{II} complexes of these hybrid thiosemicarbazonato-pyridylhydrazide ligands could form a useful platform to prepare targeted Cu radiopharmaceuticals that incorporate Aβ plaque targeting groups.[31] In an effort to develop copper complexes for the diagnostic imaging of Alzheimer's disease we have synthesized hybrid thiosemicarbazonato-pyridylhydrazide tetradentate ligands that incorporate Aβ plaque targeting styrylpyridine and benzothiazole functional groups (Figure 2). Preliminary biodistribution studies in mice showed that the brain uptake of $^{64}Cu^{II}\mathbf{L}^2$ (R = CH_3, Figure 2) was very low so a derivative with a $-(CH_2)_2N(CH_3)_2$ functional group capable of forming an intramolecular hydrogen bond ($Cu^{II}\mathbf{L}^3$) was prepared with a view to improving brain uptake.

RESULTS

Synthesis and Characterization. The benzothiazole ^{11}C-PIB was the structural inspiration behind the preparation of $H_2\mathbf{L}^1$. The acid chloride of 2-chloronicotinic acid was cyclized to the benzothiazole by condensation with 2-aminothiophenol to give 2-chloropyridinyl-4-benzothiazole (Scheme 1). Substitution of the aromatic chloride with hydrazine in refluxing ethanol resulted in the precipitation of light yellow 2-hydrazinopyridinyl-4-benzothiazole in near quantitative yield. The substituted hydrazine reacts with diacetyl-mono-4-methyl-3-thiosemicarbazone in ethanol to give $H_2\mathbf{L}^1$ in good yield (76%) and high purity. The electrospray mass spectrum (ESMS) and NMR spectra were consistent with the proposed structure, and purity was confirmed by reverse phase high-performance liquid chromatography (RP-HPLC) and microanalysis. Two new tetradentate ligands featuring *p*-dimethylaminostyryl-2-pyridylhydrazone functional groups, $H_2\mathbf{L}^2$ and $H_2\mathbf{L}^3$, were also prepared. The synthesis of 2-chloropyridinyl-4-methylenediethyl-phosphonate was achieved by reducing 2-chloronicotinic acid with lithium aluminum hydride to furnish the corresponding alcohol, followed by chlorination with thionylchloride and an Arbuzov rearrangement with triethylphosphite to give diethylphosphonate **1** (Scheme 2). A Horner-Wadsworth coupling between diethylphosphonate (**1**) and aldehyde 4,4-dimethylbenzaldehyde formed styrylpyridine derivative (**2**) in good yield. Treatment of **2** with hydrazine hydrate allowed isolation of **3**, and the synthesis of $H_2\mathbf{L}^2$ was fulfilled by condensation between **3** and diacetyl-mono-4-

dx.doi.org/10.1021/ja4057807 | J. Am. Chem. Soc. 2013, 135, 16120−16132

Scheme 1. Synthesis of H_2L^1 and $Cu^{II}L^1$

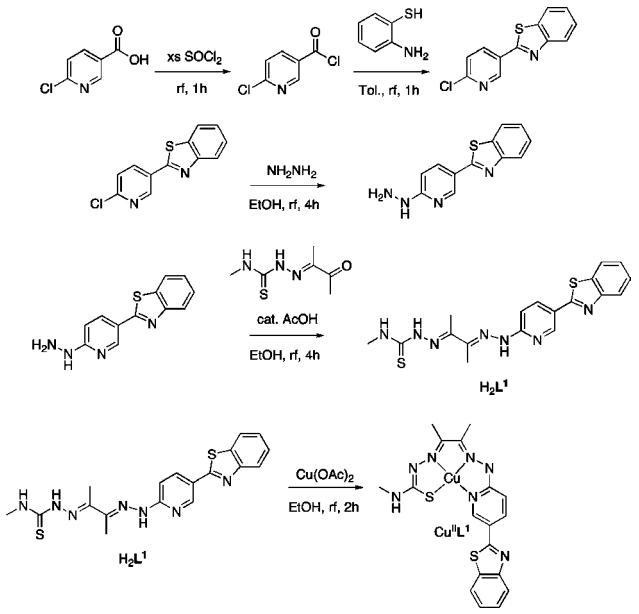

Scheme 2. Synthesis of H_2L^2 and $Cu^{II}L^2$

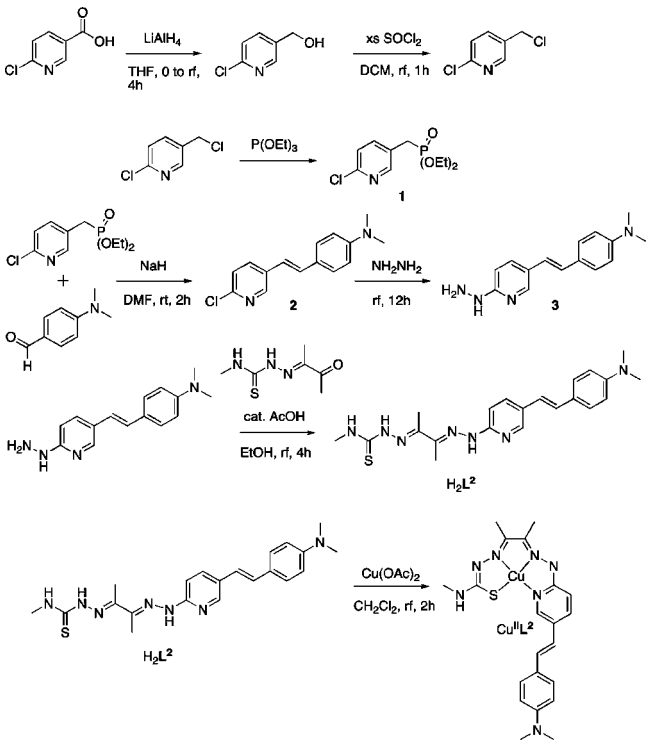

methyl-3-thiosemicarbazone in ethanol (Scheme 2). H_2L^2 was characterized by ESMS and NMR spectroscopy, with the ^1H NMR spectrum displaying a single isomer with the expected AB splitting pattern ($^3J_{HH}$ = 16 Hz) indicative of the *E*-conformation about the double bond of the stilbene. The purity of H_2L^2 was confirmed by RP-HPLC, ESMS, and microanalysis.

Preliminary biodistribution studies revealed poor brain uptake for $Cu^{II}L^2$ (*vide infra*), so a second ligand featuring a styrylpyridine functional group, H_2L^3, with a terminal *N,N*-dimethylaminoethyl substituent (Scheme 3) was also prepared. It was hoped that the addition of a functional group capable of

Scheme 3. Synthesis of H_2L^3 and $Cu^{II}L^3$

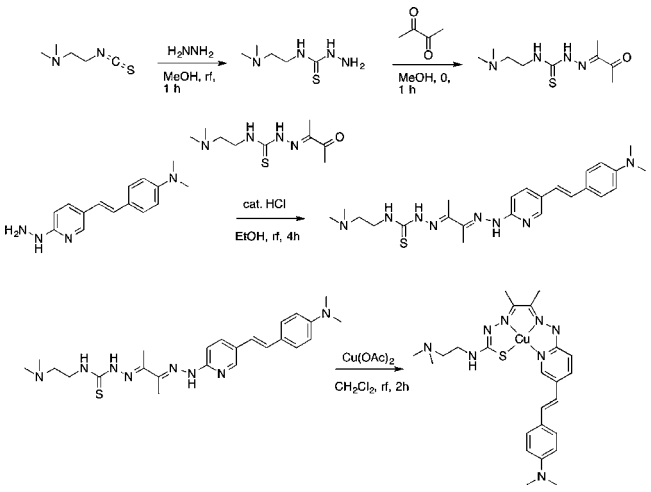

forming an intramolecular hydrogen bond would increase blood-brain barrier permeability by altering solvation. The reaction of *N,N*-dimethylethylenediamine with carbon disulfide in the presence of dicyclohexylcarbodiimide allowed isolation of isothiocyanate **4**. This isothiocyanate reacts with hydrazine to give thiosemicarbazide **5** in near quantitative yield. Dropwise addition of a solution of **5** to an excess of cooled 2,3-butanedione in methanol furnished the key mono-thiosemicarbazone **6**. The synthesis of H_2L^3 was completed by a condensation reaction to give H_2L^3 in moderate yield (Scheme 3). H_2L^3 was characterized by ESMS and NMR spectroscopy, with the ^1H NMR spectrum also displaying a single isomer with the expected AB splitting pattern ($^3J_{HH}$ = 16 Hz) indicative of the *E*-conformation about the double bond of the stilbene as seen for H_2L^2. The purity of H_2L^3 was confirmed by RP-HPLC and microanalysis.

Proligands H_2L^{1-3} react with copper acetate in either ethanol or dichloromethane to give neutral Cu^{II} complexes. The two equivalents of acetate in $Cu(CH_3CO_2)_2{\cdot}H_2O$ are sufficiently basic to doubly deprotonate the ligands. Complexation of Cu^{II} is apparent immediately after the addition of the metal salt indicated by an immediate color change and precipitation of purple $Cu^{II}L^1$ and dark blue $Cu^{II}L^2$ and $Cu^{II}L^3$. All complexes revealed an ESMS peak at the *m/z* value corresponding to $[Cu^{II}L + H^+]^+$ with the expected isotope pattern and gave a single peak when analyzed by HPLC.

The neutral $Cu^{II}L^x$ complexes are difficult to crystallize, but structural insights can be gained by crystallizing the mono cationic $[Cu^{II}(HL^x)]^+$ complexes as tetrafluoroborate salts that were isolated by slow aerial oxidation of their analogous $[Cu^{I}(H_2L^x)]^+$ complexes (*vide infra*). In the case of the Cu^{I} complexes the ligand remains neutral. Oxidation from Cu^{I} to Cu^{II} enhances the acidity of the coordinated ligand promoting a single deprotonation of the ligand on the thiosemicarbazone limb, but in the absence of a base (such as acetate) the hydrazone limb remains protonated giving monocationic $[Cu^{II}HL^x]^+$ complexes. This 'oxidation of Cu^{I} complex' methodology was used to isolate $[Cu^{II}L^1]^+$ as purple crystals of a tetrafluoroborate salt suitable for single crystal X-ray studies. The Cu^{II} is in the expected four coordinate 5−5−5 (*N,N,N,S*) chelate ring system with a distorted square planar geometry (Figure 3, Table 1). An axial association to a sulfur of an adjacent molecule [Cu1−S2 = 2.803(2) Å] and $\pi-\pi$ stacking (*ca.* 3.7 Å) between the benzothiazole rings result in

dx.doi.org/10.1021/ja4057807 | J. Am. Chem. Soc. 2013, 135, 16120−16132

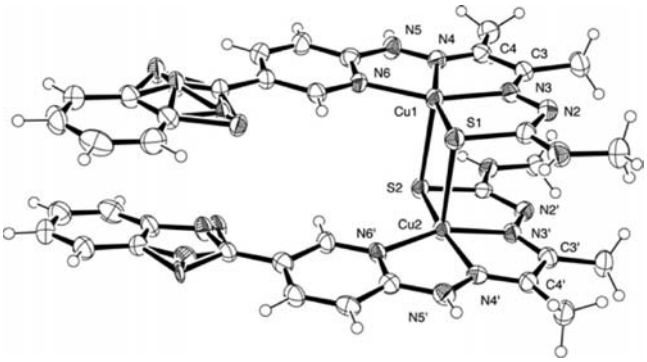

Figure 3. ORTEP (with ellipsoids at 40% probability) representation of the dication in dimer $[Cu_2^{II}(HL^1)_2](BF_4)_2{\cdot}4DMF$; benzothiazole rings are modeled as disordered over 2 sites (occupancy 0.5), with solvent molecules and anions omitted for clarity.

the formation of a dimer and a tendency toward square pyramidal geometry with the copper ≈ 0.165 Å out of the N_3S plane. The N3−Cu1−S1 bond angle (85.76(13)°) is significantly larger than the bond angle for N4−Cu1−N6 (80.70(16)°) and deprotonation of the thiosemicarbazonato limb is reflected in the C2−S1 distance of 1.773(4) Å and the C2−N2 distance of 1.333(6) Å.[31]

Dark blue crystals of $[Cu^{II}(HL^2)]BF_4$ suitable for analysis by single crystal X-ray crystallography were isolated by slow aerial oxidation of $[Cu^{I}(H_2L^2)_2]^{2+}$ (*vide infra*) and revealed a centrosymmetric dimer (Figure 4, Table 1). The double bond retains the *E*-conformation and is disposed in a *syn* arrangement to the nitrogen of the pyridyl group. Once again the Cu^{II} is bound with the expected N3S donor set and in a distorted square planar geometry tending toward square pyramidal with weak axial interaction with the sulfur of an adjacent molecule (Cu1−S1 of 2.7930(6) Å) marginally shorter than observed for $[Cu_2^{II}(HL^1)_2](BF_4)_2$ and the Cu^{II} resides slightly further out of the N_3S plane (∼0.179 Å). The trend in internal bond angles and distances in the chelate ring is analogous to $[Cu_2^{II}(HL^1)_2](BF_4)_2$ with the chelate angle for N4−Cu1−N6 (80.33(7)°) notably smaller than N3−Cu1−S1 (99.24(5)°), reflecting the elongated 'thiolate-like' C2−S1 bond length of 1.776 Å of the deprotonated thiosemicarbazonato limb.

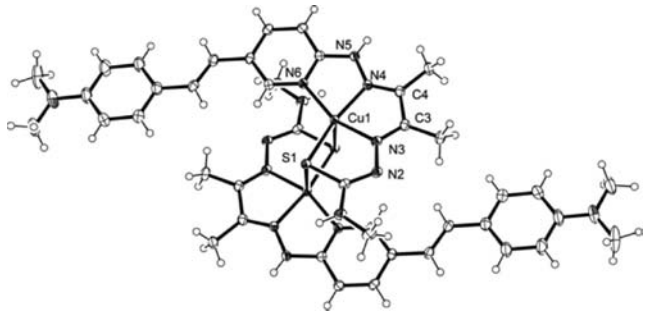

Figure 4. ORTEP (40% probability ellipsoids) representation of the cation in $[Cu^{II}(H_2L^2)]BF_4{\cdot}2DMF$, with solvent molecules and anion omitted for clarity.

It was also possible to isolate an air sensitive Cu^{I} complex of H_2L^2. Red crystals of $[Cu^{I}_2(H_2L^2)_2](BF_4)_2$ were characterized by single crystal X-ray crystallography (Figure 5, Table 1). The

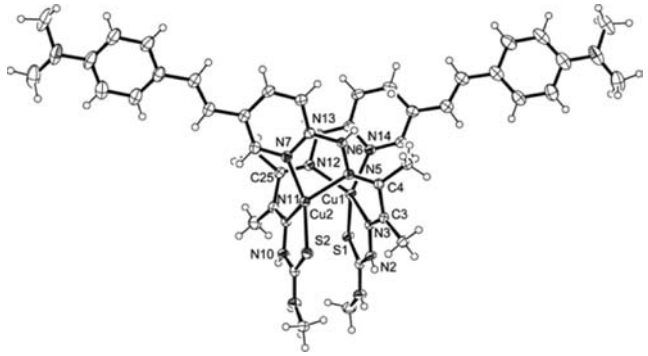

Figure 5. ORTEP (40% probability) representation of cationic helical dimer $[Cu^{I}_2(H_2L^2)_2]^{2+}$, with solvent molecules and anions omitted for clarity.

complex has two ligands bridging two Cu^{I} atoms, with each ligand binding in a bidentate N−S to one Cu^{I} atom and $N-N_{py}$ to the other Cu atom. Significant torsion about the C−C ligand backbone (N3−C3−C4−N5 = 46.6(3)° and N11−C24−C25−N12 = 48.6(3)°) permits a distorted tetrahedral geometry for each Cu^{I} ion, with the distance between copper atoms Cu−Cu

Table 1. Crystallographic Data

	$[Cu^{II}_2(HL^1)_2](BF_4)_2{\cdot}4DMF$	$[Cu^{I}_2(H_2L^2)_2](BF_4)_2{\cdot}4DMF$	$[Cu^{II}(HL^2)]BF_4{\cdot}2DMF$
Chemical formula	$C_{48}H_{64}B_2Cu_2F_8N_{18}O_4S_4$	$C_{54}H_{84}B_2Cu_2F_8N_{17}O_4S_2$	$C_{27}H_{40}BCuF_4N_9O_2S$
M	1386.11	1400.20	705.09
Crystal system	triclinic	monoclinic	monoclinic
Space group	*P*-1	$P2_1/n$	$P2_1/c$
a/Å	14.4906(10)	14.45020(10)	10.04100(10)
b/Å	14.7853(8)	29.0584(2)	8.78070(10)
c/Å	16.6716(10)	15.50960(10)	36.4738(5)
α/°	109.313(5)	90.00	90.00
β/°	115.113(6)	95.7430(10)	96.7350(10)
γ/°	93.167(5)	90.00	90.00
V/Å^3	2971.2(3)	6479.79(8)	3193.59(7)
T/K	130(2)	130(2)	130(2)
Z	2	4	4
N_{ind}	10694	11685	5740
R_{int}	0.0608	0.0241	0.0501
$R(I > 2\sigma(I))$	0.0547	0.0404	0.0402
w*R*(all data)	0.1394	0.1078	0.1033

dx.doi.org/10.1021/ja4057807 | *J. Am. Chem. Soc.* 2013, 135, 16120−16132

(3.398 Å) suggesting little interaction but resulting in the ligands adopting a helical conformation. Unlike the Cu^{II} complexes the ligand remains protonated, as suggested by the 'thione-like' bond lengths of 1.693(2) Å for C2−S1 and 1.698(2) Å for C23−S2.[31−33]

Electrochemistry and Electronic Spectroscopy. The $Cu^{II/I}$ reduction potential of each of the complexes was measured by cyclic voltammetry. The *N,N*-dimethylaminostyrylpyridine functional group present in $Cu^{II}L^2$ and $Cu^{II}L^3$ results in a lower reduction potential −0.68 V vs SCE (ΔE = 0.09 V, I_c/I_a = 1.03 and ΔE = 0.10 V, I_c/I_a = 1.04), when compared to the benzothiazole functionalized compound in $Cu^{II}L^1$, E_m = −0.58 V vs SCE (ΔE = 0.07 V, I_c/I_a = 1.07) (Figure 6). Under

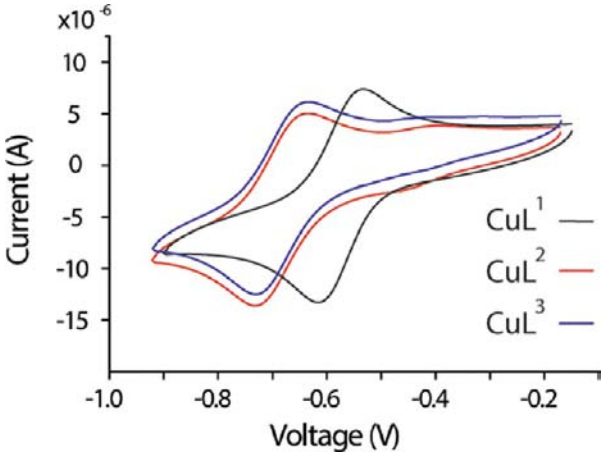

Figure 6. Cyclic voltammograms of $Cu^{II}L^{1-3}$. Scan rate 0.1 V s^{-1}. Potentials are quoted relative to a SCE.

the same conditions Fc/Fc^+: E_m = 0.53 V (ΔE = 0.158 V, I_c/I_a = 1.29) and Cu^{II}(atsm) E_m = −0.59 V (ΔE = 0.08 V, I_c/I_a = 0.89). Given that Cu^{II}(atsm) is sufficiently stable for imaging applications the measured reduction potentials suggest that $Cu^{II}L^{1-3}$ will be resistant to reductively assisted loss of the metal ion from the ligand.

The complexes $Cu^{II}L^{1-3}$ display similar electronic spectra to each other in acetonitrile (Figure S1, Supporting Information), with ligand based absorbances centered at λ_{abs} = 300 nm ($Cu^{II}L^1$, ε = 1.8 × 10^4 M^{-1} cm^{-1}, $Cu^{II}L^2$, ε = 3.2 × 10^4 M^{-1} cm^{-1}, $Cu^{II}L^3$, ε = 2.0 × 10^4 M^{-1} cm^{-1}) and λ_{abs} = 380 nm ($Cu^{II}L^1$, ε = 1.5 × 10^4 M^{-1} cm^{-1}, $Cu^{II}L^2$, ε = 3.8 × 10^4 M^{-1} cm^{-1}, and $Cu^{II}L^3$, ε = 1.9 × 10^4 M), along with a broad absorbance between λ_{abs} = 500−650 nm ($Cu^{II}L^1$ λ_{580}, ε = 8 × 10^3 M^{-1} cm^{-1}, $Cu^{II}L^2$ λ_{620}, ε = 1.2 × 10^4 M^{-1} cm^{-1}, and $Cu^{II}L^3$ λ_{640}, ε = 7.2 × 10^3 M^{-1} cm^{-1}) characteristic of metal to ligand charge transfer (MLCT) transitions. Ligands H_2L^{1-3} are fluorescent displaying a broad emission centered at λ_{em} = 480 nm (λ_{ex} = 390 nm). Coordination of paramagnetic d^9 Cu^{II} results in a reduction in the fluorescent intensity, but the copper complexes are still fluorescent. $Cu^{II}L^1$ displays a broad emission centered at λ_{em} = 420 nm (λ_{ex} = 370 nm). $Cu^{II}L^2$ and $Cu^{II}L^3$ fluoresce at λ_{em} = 480 nm and λ_{em} = 465 nm, respectively (λ_{ex} = 390 nm).

The stability of metal complexes in the presence of glutathione is often used as a ligand and redox challenge to predict *in vivo* stability of complexes used for radiopharmaceuticals.[34] The characteristic MLCT and ligand-based absorbances were used to monitor the stability of the complex $Cu^{II}L^2$ by RP-HPLC in the presence of glutathione (GSH). A degassed solution of $Cu^{II}L^2$ (100 μM) was incubated in the presence of 100-fold GSH (30% DMSO/phosphate buffer 20 mM, pH 7.4) over 4 h at 37 °C, with aliquots analyzed by RP-HPLC measuring the MLCT absorption. There was no significant change suggesting that $Cu^{II}L^2$ is sufficiently stable in the presence of GSH. Further prediction of likely in vivo metabolism of these copper complexes could involve an assessment of their stability in liver microsomes and in the presence of disease relevant concentrations of H_2O_2.[35−39]

Titration of either H_2L^2 or H_2L^3 with Cu^{II} in 30% DMSO/PB (20 mM, pH 7.4) induces the characteristic intense MLCT absorbance and color observed for the neutral coordination complexes isolated using $Cu(CH_3CO_2)_2{\cdot}H_2O$ as both a base and a source of Cu^{II}, suggesting that at pH 7.4 the Cu^{II} is coordinated to a dianionic tetradentate ligand framework (Figure S2). When a solution of H_2L^3 was titrated with Cu^{II} in 30% DMSO/PB (20 mM, pH 7.4) an absorbance emerged in the visible range (λ_{550}, ε = 1.1 × 10^4 M^{-1} cm^{-1}) with an isosbestic point at 450 nm (Figure S2). A similar absorption is obtained at pH 6.5 (30% DMSO/MES 20 mM). A plot of A_{550} vs [Cu^{II}]/[H_2L^3] ratio produced a straight line with a sharp turning point at 1.0, confirming that the ligand converts to a monomeric complex with a likely high binding affinity.[40] The K_D of H_2L^3 for Cu^{II} was estimated by competition with Na_2H_2EDTA (EDTA = ethylenediaminetetraacetate, K_D = 1.10 × 10^{-16} M at pH 7.4 and K_D = 7.88 × 10^{-14} M at pH 6.5).[40] Electronic spectroscopy was used to measure competitive equilibria between a solution of $Cu^{II}L^3$ and increasing equivalents of EDTA (Figure S3). The data from a series of experiments with varying Cu^{II} occupancies on both ligands were used to generate apparent conditional dissociation constant of H_2L^3 for Cu^{II}: K_D = 5.8(4) × 10^{-18} M at pH 7.4 and K_D = 1.7(2) × 10^{-15} M at pH 6.5 (Figure S3 and Table S1/S2). Preliminary experiments with H_2L^2 suggested it has a similar affinity for Cu^{II} as H_2L^3. The Aβ(1−42) peptide is known to form complexes with Cu^{II} the binding affinity of these complexes is in dispute but is perhaps close to a K_D = 10^{-10} M.[40−43] The Cu^{II} binding fragment is within the Aβ(1−16) fragment of the peptide.[44,45] Addition of Aβ(1−16) to a solution of $Cu^{II}L^3$ did not result in any change to the electronic spectrum indicating that Aβ(1−16) peptide is not able to displace Cu^{II} from the tetradentate ligand.

Interaction of $Cu^{II}L^{1-3}$ with Aβ Plaques in Human Brain Tissue. Human brain tissue (5 μm serial sections) was pretreated with bovine serum albumin to prevent nonselective binding and then treated with solutions of $Cu^{II}L^{1-3}$ (50 μM in 15% DMSO/PB, 20 mM, pH 7.4). The localization of $Cu^{II}L^{1-3}$ on the treated brain tissue was measured by epi-fluorescent microscopy (λ_{ex} = 359 nm, λ_{em} = 461 nm) and compared to the contiguous section immuno-stained with an Aβ antibody (1E8) to identify plaques. Aβ plaques are typically 40−60 μm in diameter, such that 5 μm serial sections would comprise the same Aβ plaque.[46] Compound $Cu^{II}L^1$ suffered from very poor solubility in the media used for the experiment and did not appear to selectively interact with Aβ plaques. In contrast, for both $Cu^{II}L^2$ (Figure 7) and $Cu^{II}L^3$ (Figure 8) colocalization of the immuno-stained plaques and the copper complexes is clearly evident demonstrating that the new compounds are binding to Aβ plaques in human brains. Importantly, both compounds are not retained in the age-matched control tissue. The metal free ligands H_2L^2 and H_2L^3 also bind to Aβ plaques in human brain tissue (Figure S5).

dx.doi.org/10.1021/ja4057807 | J. Am. Chem. Soc. 2013, 135, 16120−16132

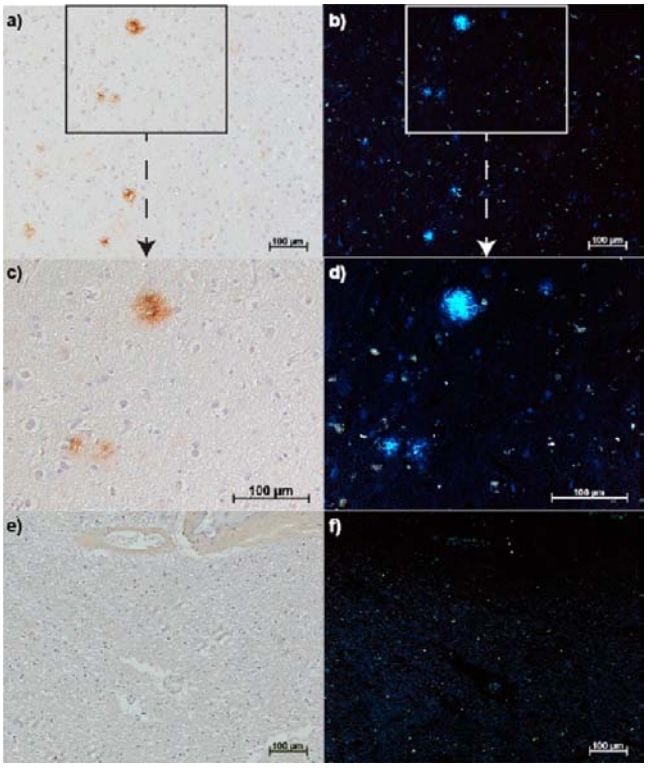

Figure 7. AD human brain sections with 1E8 antibody stained Aβ plaques (a) × 10, (c) × 20 magnification; and epi-fluorescence microscopy of $Cu^{II}L^2$ binding to Aβ plaques (b) × 10, (d) × 20 magnification measured at λ_{ex} = 359 nm, λ_{em} = 461 nm; controls consist of age-matched healthy brain sections treated with (e) 1E8 antibody and (f) $Cu^{II}L^2$.

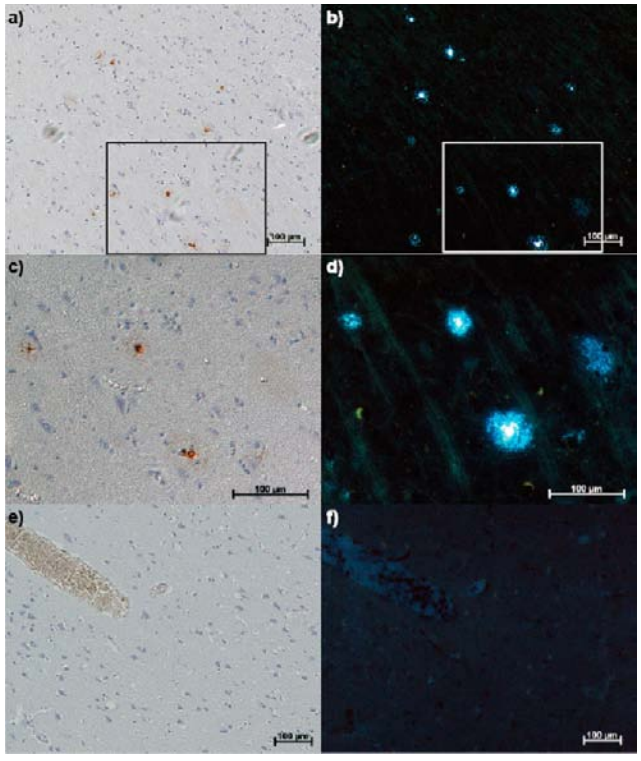

Figure 8. AD human brain sections with 1E8 antibody stained Aβ plaques (a) × 10, (c) × 20 magnification; and epi-fluorescence microscopy of $Cu^{II}L^3$ binding to Aβ plaques (b) × 10, (d) × 20 magnification measured at λ_{ex} = 359 nm, λ_{em} = 461 nm; controls consist of age-matched healthy brain sections treated with (e) 1E8 antibody and (f) $Cu^{II}L^3$.

Radiolabeling with ^{64}Cu and Biodistribution in Mice. Both $^{64}Cu^{II}L^2$ and $^{64}Cu^{II}L^3$ were prepared in ~95% radiochemical purity by the addition of $^{64}Cu^{II}Cl_2$ (dissolved in 0.1 M HCl to mixtures of H_2L^2 or H_2L^3 in PBS buffer (0.01 M, pH 7.4). The identity of the radiolabeled product was confirmed by comparison of the HPLC profiles of the nonradioactive analogues (Figure 9). The distribution coefficients (log *D*, pH 7.4) were measured to be 1.90 for $Cu^{II}L^2$ and 1.87 for $Cu^{II}L^3$ and were comparable to that of Cu^{II}(atsm) (1.85).

Micro-PET images in wild-type mice (Balb/c) following intravenous tail injection of either $^{64}Cu^{II}L^2$ or $^{64}Cu^{II}L^3$ (~13 MBq) were acquired 5 min postinjection. The images revealed that little $^{64}Cu^{II}L^2$ can be observed in brain at this time point but images acquired using $^{64}Cu^{II}L^3$ were more encouraging with a significant amount of activity observed in the brain (Figure 10). The brain uptake of $^{64}Cu^{II}L^3$ was quantified by biodistribution experiment in normal mice (Table 2). $^{64}Cu^{II}L^3$ displayed good uptake (1.11% ID/g) at 2 min post injection dropping to 0.38% ID/g at 30 min. This indicates $^{64}Cu^{II}L^3$ can rapidly cross the blood-brain barrier of normal mice with a highly desirable fast washout from the brain as anticipated with no Aβ plaques to trap the imaging agent. Distribution in remaining organs suggests initial high uptake in the lungs and spleen (Table 2).

DISCUSSION

The versatility offered by the range of different positron-emitting copper isotopes means that the element has quite unique potential for diagnostic PET imaging.[22,23] There are two

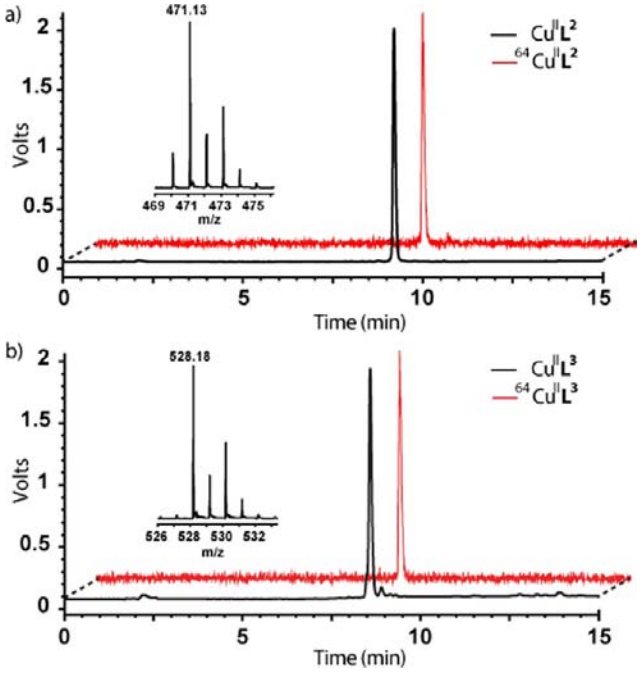

Figure 9. (a) HPLC of $^{64}Cu^{II}L^2$ (offset by 1 min) with detection of radioactivity compared with nonradioactive $Cu^{II}L^2$ (UV detection at 280 nm) and inset ES-MS of $[Cu^{II}L^2 + H^+]$; (b) HPLC of $^{64}Cu^{II}L^3$ (offset by 1 min) with detection of radioactivity compared with 'nonradiaoctive' $Cu^{II}L^3$ (UV detection at 280 nm) and inset ES-MS of $[Cu^{II}L^3 + H^+]$.

dx.doi.org/10.1021/ja4057807 | J. Am. Chem. Soc. 2013, 135, 16120−16132

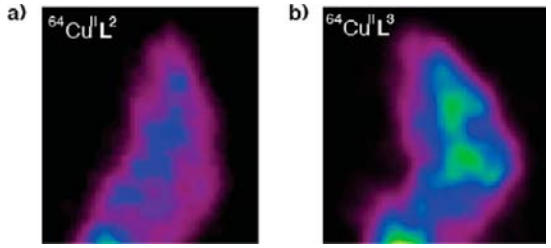

Figure 10. 3D collated micro-PET image of the head of Balb/c mice, following intravenous injection of (a) $^{64}Cu^{II}L^2$ and (b) $^{64}Cu^{II}L^3$.

Table 2. Biodistribution of Radioactivity after Injection of $^{64}Cu^{II}L^3$ in Balb/c Mice

	%ID/g	
Tissue	2 m.p.i.	30 m.p.i.
Blood	4.25(0.56)	1.70(0.29)
Lungs	42.16(20.27)	17.74(4.55)
Heart	12.08(1.50)	5.26(0.86)
Liver	11.28(5.02)	7.38(0.59)
Kidneys	15.25(2.02)	5.17(0.63)
Muscle	0.51(0.50)	0.90(0.13)
Spleen	18.02(3.35)	8.24(0.89)
Brain	**1.11(0.20)**	**0.38(0.09)**

[a]Each value represents the mean (SD) for three animals expressed as % injected dose per gram, m.p.i. = minutes post injection.

comparatively short-lived isotopes, copper-60 ($t_{1/2}$ = 20 min) which is relatively easy to produce with a small medical cyclotron and copper-62 ($t_{1/2}$ = 20 min), which is available from a convenient generator. Two longer half-life isotopes are also accessible, copper-61 ($t_{1/2}$ = 3.4 h) and copper-64 ($t_{1/2}$ = 12.7 h) can both be produced in low energy hospital cyclotrons.[22] The low energy of the positron-emission from copper-64 coupled to the lack of interfering gamma emissions means that the images obtained are comparable to those obtained with fluorine-18.[47] A single ligand framework is suitable for the full range of copper isotopes and would serve as a valuable platform to develop versatile Aβ plaque imaging agents and improve the number of clinical centers that are capable of assessing Aβ plaque burden in patients.

A family of ligands known as bis(thiosemicarbazones), derived from 1,2-diones, continue to be of interest as delivery vehicles for radioactive copper isotopes as they form stable (K_a = 10^{18}) and neutral membrane permeable copper complexes.[48−52] The copper complex $^{64}Cu^{II}$(atsm) (Figure 2) is currently undergoing clinical trials for imaging hypoxia in head and neck cancers.[27,28,32,53] Of particular significance to this study is that the neutral, lipophilic bis(thiosemicarbazonato)-Cu^{II} complexes cross the blood-brain barrier and have been used for PET imaging of the brain.[54−58]

The demonstrated success of the bis(thiosemicarbazonato) Cu^{II} framework for brain imaging inspired the synthesis of the hybrid thiosemicarbazone-benzothiazole and thiosemicarbazone-styrylpyridine tetradentate ligands H_2L^{1-3}. All three ligands formed stable complexes with Cu^{II}, and $Cu^{II}HL^1$ and $Cu^{II}HL^2$ were characterized by single crystal X-ray crystallography. Electronic spectroscopy showed that all the complexes were charge-neutral in aqueous buffer at pH 7.4. The ligands form stable complexes with Cu^{II} and for $Cu^{II}L^3$ the conditional dissociation constant (K_D) is 5.8(4) × 10^{-18} M at pH 7.4 and 1.7(2) × 10^{-15} M at pH 6.5. The stability at the lower pH was measured as Alzheimer's disease can be complicated by cerebral acidosis (pH 6.6).[59,60]

The $Cu^{II/I}$ reduction potentials of bis(thiosemicarbazonato)-Cu^{II} complexes can be used to predict intracellular reduction and stability *in vivo*.[53,61,62] The quasi-reversible $Cu^{II/I}$ couples are predominantly metal-based, but it is recognized that the conjugated ligand is not entirely 'innocent'.[63] The hypoxia selectivity of Cu^{II}(atsm) is thought to be a consequence of the neutral complex diffusing into all cells but only being trapped in hypoxic cells by virtue of reduction of the Cu^{II} to Cu^{I} and the lower oxidizing potential of hypoxic cells preventing reoxidation. Cyclic voltammetry measurements in DMF of the neutral complexes $Cu^{II}L^{1-3}$ show that all the complexes undergo quasi-reversible reduction attributed to a Cu^{II}/Cu^{I} couple at more negative potentials than the corresponding reduction in Cu^{II}(atsm). The two compounds with *N,N*-dimethylaminostyrylpyridine functional groups, $Cu^{II}L^2$ and $Cu^{II}L^3$, have a lower $Cu^{II/I}$ reduction potential than the benzothiazole containing compound, $Cu^{II}L^1$. Presumably the electron donating effects of the *N,N*-dimethylamine functional group are effectively transmitted throughout the conjugated ligand which results in a more negative reduction potential.

The complexes that incorporated a functionalized styrylpyridine plaque-targeting group, $Cu^{II}L^2$ and $Cu^{II}L^3$, bind to Aβ plaques in human brain tissue. In the case of $Cu^{II}L^2$ there is evidence that the compound binds selectively to the fibrillar plaques present in this particular sample (Figure 7).[64] $Cu^{II}L^3$ demonstrates significant binding to the core plaques as well as more diffuse plaques present in the sample of tissue examined (Figure 8).

Metal chelators that can redistribute metal ions bound to Aβ plaques are of interest as potential therapeutics.[36,65−73] Perhaps the most studied compounds of this class are hydroxyquinoline chelators that have been trialed in human AD subjects.[74,75] The metal free ligands H_2L^2 and H_2L^3 bind to Aβ plaques in human brain tissue (see Figure S5). As chelators with some degree of specificity for Cu^{II} and Zn^{II}, H_2L^2 and H_2L^3 could be of interest as potential therapeutics.

Both $Cu^{II}L^2$ and $Cu^{II}L^3$ were radiolabeled in high radiochemical yield in a single step at room temperature in phosphate buffer. As a measure of lipophilicity log *D* values are of some use in predicting the ability of compounds to cross the blood-brain barrier.[76,77] The log *D* values measured for $Cu^{II}L^2$ (1.90) and $Cu^{II}L^3$ (1.87) were comparable to that of Cu^{II}(atsm) (1.85) and within suggested optimum values for penetration of the central nervous system. The binding of $Cu^{II}L^2$ and $Cu^{II}L^3$ to Aβ plaques in human brain tissue was encouraging and when coupled to the ease of the radiochemical synthesis warranted further investigation of the ability of the compounds to cross the blood-brain barrier. Preliminary micro-PET studies in wild-type mice following administration of $^{64}Cu^{II}L^2$ were disappointing with essentially no radioactivity evident in the brain five minutes postinjection. The images obtained following administration of $Cu^{II}L^3$ were much more promising with significant radioactivity observable in the brain (Figure 10). These differences were quantified by a biodistribution study that revealed that at five minutes post injection 1.11 (0.20) %ID/g had accumulated in the brain, and in wild-type mice, the radioactivity cleared to 0.38 (0.09) %ID/g 30 min post injection. These levels of brain uptake are comparable to Cu^{II}(atsm) in wild-type mice (0.9 (0.4) %ID/g).[39] The brains of these animals are not expected to possess Aβ plaques, so this clearance from nontarget tissue is a

dx.doi.org/10.1021/ja4057807 | J. Am. Chem. Soc. 2013, 135, 16120−16132

desirable feature. The fact that $Cu^{II}L^2$ displays no brain uptake but $Cu^{II}L^3$ shows significant uptake within the brain highlights the challenges in designing metal complexes that cross the brain capillary endothelial cells with tight junctions that form the blood-brain barrier. The two compounds have similar lipophilicity as measured by log *D* values, so this often used parameter does not provide insight into their differing abilities to enter the central nervous system. Lipophilic compounds often display high levels of deposition in the lungs, liver, and spleen, as well as being susceptible to metabolism by P450 enzymes. This, coupled to nonspecific binding to albumin and other serum proteins, can decrease the dose of a particular tracer that enters the brain. Another potential complication is that the blood-brain barrier contains efflux pumps including the p-glycoprotein that act to remove substrates from the brain. There is reduced cellular retention and higher levels of efflux of the related compounds $^{64}Cu^{II}$(atsm) and $^{64}Cu^{II}$(ptsm) in cell-lines that highly express p-glycoprotein (MDR1).[78,79] The inability of $Cu^{II}L^2$ to cross the blood-brain barrier led to the judicious choice of adding a terminal $-(CH_2)_2N(CH_3)_2$ functional group to the ligand framework to give $Cu^{II}L^3$. Although this substitution increased the molecular weight of the complex, it was hoped that the addition of a functional group capable of forming an intramolecular hydrogen bond that has the potential to alter the aqueous solvation via H-bond interactions with solvent might increase blood-brain barrier permeability.[80] In this case the strategy was successful. It is also possible that the added functional group in $Cu^{II}L^3$ reduces other complicating interactions such as efflux *via* p-glycoprotein or other hydrophobic interactions with serum protein that could be limiting the brain uptake of $Cu^{II}L^2$.

CONCLUDING REMARKS

Here we have presented the synthesis of new hybrid thiosemicarbazone-pyridylhydrazine ligands with appended functional groups designed to bind to Aβ plaques. The tetradentate ligands form stable four-coordinate complexes with Cu^{II}. $Cu^{II}L^2$ and $Cu^{II}L^3$ with plaque targeting *N,N*-dimethylstyrylpyridine functional groups bind to Aβ plaques in post-mortem human brain tissue collected from subjects with AD. Both H_2L^2 and H_2L^3 can be radiolabeled with ^{64}Cu in a single and simple step to give products with a high radiochemical yield. Subtle modification of the ligand framework and the incorporation of a $-(CH_2)_2N(CH_3)_2$ functional group improved the brain uptake with preliminary studies of biodistribution in normal mice revealing that $^{64}Cu^{II}L^3$ can rapidly cross the blood-brain barrier and displays a highly desirable fast washout from the brain. Future experiments will investigate the uptake of these compounds in transgenic mouse models of amyloid pathology. The work presented here offers some insight into strategies to both target Aβ plaques and modify the biodistribution of metal complexes. The styrylpyridine functional groups present in $Cu^{II}L^2$ and $Cu^{II}L^3$ retain the ability to bind to Aβ plaques despite the pyridyl functional group being involved in coordination to a metal ion.

The intermediate half-life of ^{64}Cu enables PET imaging using this radioisotope to be carried out at a site remote from the cyclotron facility used to generate the radionuclide. There is an increasing requirement for PET radiopharmaceuticals to comply with good manufacturing practices (GMP). The quality assurance procedures necessary to meet GMP requirements can be challenging with tracers that feature radionuclides with short half-lives. The relatively slow physical decay of ^{64}Cu when compared to ^{18}F and ^{11}C would allow performance quality assurance procedures during transport from a centralized radiopharmacy to a number of PET centers. It is envisaged that the new ligands could readily be incorporated into 'kit' formulations in a similar manner to the successful technetium-99m based radiopharmaceuticals that play a major role in noninvasive imaging with single photon emission computed tomography. This study has focused on ^{64}Cu but the ligands would also be suitable for the other positron-emitting isotopes of copper offering incredible versatility and flexibility from a platform with the potential to increase the feasibility of performing noninvasive diagnostic imaging of AD at more hospitals.

EXPERIMENTAL SECTION

Crystallography. Crystals of $[Cu_2^{II}(HL^1)_2](BF_4)_2$, $[Cu^{I}_2(H_2L^2)](BF_4)_2$, and $[Cu^{II}(HL^2)]BF_4$, respectively, were mounted in low temperature oil then flash cooled to 130 K using an Oxford low temperature device. Intensity data were collected at 130 K with an Oxford XCalibur X-ray diffractometer with Sapphire CCD detector using Cu−Kα radiation (graphite crystal monochromator λ = 1.54184 Å). Data were reduced and corrected for absorption. The structures were solved by direct methods and difference Fourier synthesis using the SHELX suite of programs as implemented within the WINGX[2,3,38] software. Thermal ellipsoid plots were generated using the program ORTEP-3 integrated within the WINGX suite of programs.

General Procedures. *Syntheses.* All reagents and solvents were obtained from commercial sources (Sigma-Aldrich) and used as received unless otherwise stated. Diacetyl-mono-4-methyl-3-thiosemicarbazone was prepared according to previous reports. Elemental analyses for C, H, and N were carried out by Chemical & MicroAnalytical Services Pty. Ltd., Vic. NMR spectra were recorded on a Varian FT-NMR 500 spectrometer (^{1}H NMR at 499.9 MHz and $^{13}C\{^1H\}$ NMR at 125.7 MHz) or an Agilent MR 400 spectrometer (^{1}H NMR at 399.9 MHz) at 298 K, and referenced to the internal solvent residue. Mass spectra were recorded on an Agilent 6510-Q-TOF LC/MS mass spectrometer and calibrated to internal references.

UV/visible Spectroscopy. UV/vis spectra were recorded on either a Cary 300 Bio UV−vis spectrophotometer or a Shimadzu UV-1650 PC spectrophotometer, from 800 to 250 at 0.5 nm data intervals with a 600 nm/min scan rate.

The stability of the complex $Cu^{II}L^2$ was monitored by RP-HPLC in the presence of glutathione (GSH). A degassed solution of $Cu^{II}L^2$ (100 μM) was incubated in the presence of 100-fold GSH (30% DMSO/phosphate buffer 20 mM, pH 7.4) over 4 h at 37 °C, with aliquots analyzed by RP-HPLC measuring the MLCT absorption (A_{550}).

Dissociation constants for $Cu^{II}L^3$ at various pH were determined by photometric titration measuring the change in the UV/vis spectrum (A_{550}) of a solution containing either (a) $Cu^{II}L^3$ (10 μM) in 30% DMSO/PB (20 mM, pH 7.4) upon 24 h incubation with increasing EDTA (10, 50, 100 150 μM) or (b) $Cu^{II}L^3$ (10 μM) in 30% DMSO/MES (20 mM, pH 6.5) upon 24 h incubation with increasing EDTA (10, 50, 100 150 μM) (Figure S3 and Table S1/2 in SI).

Fluorescence Spectroscopy. Fluorescence emission spectra were measured on a Varian Cary Eclipse Fluorescence spectrophotometer.

High Performance Liquid Chromatography. Analytical RP-HPLC traces were acquired using an Agilent 1200 series HPLC system equipped with a Agilent Zorbax Eclipse XDB-C18 column (4.6 × 150 mm, 5 μm) with a 1 mL/min flow rate and UV spectroscopic detection at 214 nm, 220 nm, and 270 nm. Retention times (R_t/min) were recorded using a gradient elution method of 0−100% B over 25 min, solution A consisted of water (buffered with 0.1% trifluoroacetic acid) and solution B consisted of acetonitrile (buffered with 0.1% trifluoroacetic acid).

Electrochemistry. Cyclic voltammograms were recorded using an AUTOLAB PGSTAT100 equipped with GPES V4.9 software. Measurements of the complexes were carried out at approximately 1

dx.doi.org/10.1021/ja4057807 | J. Am. Chem. Soc. 2013, 135, 16120−16132

$\times 10^{-3}$ M in dimethylformamide with tetrabutylammonium tetrafluoroborate (1×10^{-1} M) as electrolyte using a glassy carbon disk (d, 3 mm) working electrode, a Pt wire counter/auxiliary electrode, and a Ag/Ag^{+} pseudo reference electrode (silver wire in H_2O (KCl (0.1 M)) $AgNO_3$ (0.01 M)). Ferrocene was used as an internal reference ($E_m(Fc/Fc^{+})$ = 0.54 V vs SCE), where E_m refers to the midpoint between a reversible reductive (E_{pc}) and oxidative (E_{pa}) couple, given by $E_m = (E_{pc} + E_{pa})/2$. Irreversible systems are only given reductive (E_{pc}) and oxidative (E_{pa}) values, respectively.

Mass Spectroscopy. Mass spectra were recorded in the positive ion mode on an Agilent 6510 Q-TOF LC/MS Mass Spectrometer coupled to an Agilent 1100 LC system (Agilent, Palo Alto, CA). Data were acquired and reference mass corrected via a dual-spray electrospray ionization source, using the factory-defined calibration procedure. Each scan or data point on the Total Ion Chromatogram is an average of 9652 transients, producing 1.02 scans s^{-1}. Averaging the scans across each peak generated spectra. Mass spectrometer conditions: fragmentor, 200−300 V; drying gas flow, 7 L/min; nebulizer, 30 psi; drying gas temp, 325 °C; V_{cap}, 4000 V; skimmer, 65 V; OCT R_fV, 750 V; scan range acquired, 150−3000 *m*/*z*.

Staining of Human AD Brain Tissues. Paraffin preserved brain tissue blocks were provided by the Victoria Brain Bank Network. Brain tissue was collected at autopsy. The National Neural Tissue Resource Centre performed sourcing and preparation of human brain tissue. AD pathologic diagnosis was made according to standard National Institute on Aging-Reagan Institute criteria. Determination of age-matched human control (HC) cases was subject to the above criteria. The AD and HC brain tissues sections (5 μM) were first deparaffined (xylene, 3 × 2 min) followed by rehydration (soaking in a series of 100%, 90%, 70%, and 0% v/v ethanol/water). The hydrated tissue sections were washed in phosphate buffer saline (PBS, 5 min). Autofluorescence of the tissue was quenched using potassium permanganate (0.25% in PBS, 20 min) and washing with PBS (2 × 2 min) to remove the excess. The now brown-colored sections were washed with potassium metabisulfite and oxalic acid (1% in PBS) until the brown color was removed followed by washing with PBS (3 × 2 min). The sections were blocked with bovine serum albumin (2% BSA in PBS, pH 7.0, 10 min) and covered with filtered $Cu^{II}\mathbf{L}$ (50 μM in 15% v/v DMSO/PBS, 30 min). The sections were treated with BSA again to remove any $Cu^{II}\mathbf{L}$ nonspecifically bound to the tissue. Finally, the sections were washed with PBS (3 × 2 min), DI water, and mounted with nonfluorescent mounting media (Dako). Fluorescence images were visualized using a Leica (Bannockburn, IL) DM1RB microscope.

^{64}Cu Radiolabeling, Log D Measurements and Mouse Biodistribution. ^{64}Cu was produced *via* the ^{64}Ni(p,n)^{64}Cu reaction, using a custom-manufactured solid target assembly positioned externally to a Cyclone 18/9 (IBA) cyclotron.[81] The primary proton beam was degraded to 11.7 MeV energy using a graphite degrader built into a graphite collimator. The target (^{64}Ni metal, 94.8−99.07% enrichment, electroplated onto an Au foil) was housed in a custom-made aluminum cradle. Helium cooling was applied to the target holder at beam entry and chilled water at beam exit. All targets were irradiated at 40 μA, for up to 2 h. After irradiation, the ^{64}Cu was isolated from the target using ion exchange chromatography, utilizing low concentrations of HCl in alcohol solution. Final reconstitution of the ^{64}Cu fraction yielded 1−2.6 GBq of ^{64}Cu as $^{64}CuCl_2$ (radionuclidic purity 99%).

General Procedure. An aliquot of $^{64}CuCl_2$ (20 μL, ∼1.5 MBq, in ∼0.02 M HCl) was added to a solution of the ligand (10 μL, 1 mg/mL DMSO) followed by a Milli-Q water tip rinse (20 μL). The reaction was left for 15 min at room temperature before addition of phosphate buffer (PB, 150 μL, 10 mM, pH 7.2). 10 μL of the reaction solution was removed and diluted to 50 μL with PB before injection and analyses by reverse-phase C18 analytical HPLC. A DMSO solution of the "cold" copper complex (1 mg/mL) was injected (10 μL) under the same conditions (λ = 280 nm) to verify the identity of the radiolabeled complex. HPLC were acquired using a Shimadzu SPD-10ATvP HPLC system equipped with a Phenomenex Luna C18 100 Å column (4.6 × 150 mm, 5 μm) with a 1 mL/min flow rate and with scintillation detector and UV−vis detector in series (280 nm). Retention times (R_t/min) were recorded using a gradient elution method of 5−100% B over 15 min, solution A consisted of water (buffered with 0.1% trifluoroacetic acid) and solution B consisted of acetonitrile (buffered with 0.1% trifluoroacetic acid).

Log D Distribution Coefficient Measurements. Octanol/PB buffer distribution coefficients were measured in triplicate by vortex mixing *n*-octanol (0.5 mL) and PB (0.5 mL, 10 mM, pH 7.2) solutions with an aliquot (40 μL) of the ^{64}Cu complex reaction. Following centrifugation, 100 μL of the *n*-octanol and aqueous phases were sampled, diluted to 1 mL and counted in an automatic well counter measuring scintillation at 511 keV. Distribution coefficients (log *D*) are reported as the log of the ratio of counts of *n*-octanol/g to counts of PB/g.

PET Imaging and Biodistribution Experiments in Mice. Age matched male wild type mice were separated into two groups for imaging and biodistribution analysis. The mice were anaesthetized using isoflurane in 50% oxygen in air before being injected intravenously with $^{64}Cu^{II}\mathbf{L}^2$ (100 μL) prepared according to the above procedure, reflecting the amount of ^{64}Cu (∼5 MBq/animal for biodistribution and ∼20 MBq/animal for imaging) required. Three animals were subsequently sacrificed at 2 min postinjection and 30 min postinjection, respectively. The organs of interest were removed and weighed, and the radioactivity was measured with an automatic counter. The percentage injected dose per gram (%ID/g) was calculated by a comparison of the tissue counts to suitably diluted aliquots of the injected material. Five minutes post injection, animals for imaging were placed on the bed of a Philips Mosaic small animal PET scanner and imaged over 10 min. The images were reconstructed using a 3D RAMLA algorithm as described previously.[82]

Synthetic Procedures. *2-Chloropyridinyl-4-benzothiazole.* 2-Chloronicotinic acid (1.00 g, 6.35 mmol) was refluxed in thionylchloride (10 mL) under nitrogen for 1 h. On cooling to room temperature, volatiles were removed *in vacuo*. The residue was treated dropwise with a solution of 2-aminothiophenol (680 uL, 6.35 mmol) in THF (50 mL) over 10−15 min, and stirred at room temperature for a further hour. The reaction was diluted with CH_2Cl_2 (20 mL) and neutralized with sat. $NaHCO_3$ (50 mL). The organic layer was separated and the aqueous washed with dichloromethane (3 × 20 mL). Organics were combined, dried over $MgSO_4$, filtered, and volatiles were removed. The residue was subsequently chromatographed (CH_2Cl_2) to give a white solid (750 mg, 48%). ^{1}H NMR (500 MHz; DMSO-d_6): δ/ppm 9.07 (d, $^4J_{HH}$ = 2.6, 1H, PyH), 8.46 (dd, $^3J_{HH}$ = 8.3, $^4J_{HH}$ =2.6, 1H, PyH), 8.18 (dt, $^3J_{HH}$ = 8, $^4J_{HH}$ = 0.6, 1H, ArH), 8.09 (dt, $^3J_{HH}$ = 8.1, $^4J_{HH}$ = 0.5, 1H, ArH), 7.57 (d, $^3J_{HH}$ = 8.4, 1H, PyH), 7.57 (ddt, $^3J_{HH}$ = 8.2, $^3J_{HH}$ = 7.2, $^4J_{HH}$ = 1, 1H, ArH), 7.50 (ddt, $^3J_{HH}$ = 8.1, $^3J_{HH}$ = 7.1, $^4J_{HH}$ = 0.9, 1H, ArH). ^{13}C{^{1}H} NMR (125.7 MHz; DMSO-d_6): δ/ppm 163.1 (BzC), 153.2 (ArC), 152.3 (PyC), 147.9 (PyCH), 137.9 (PyCH), 134.6 (ArC), 128.3 (PyCCl), 126.9 (ArCH), 126.0 (ArCH), 124.9 (PyCH), 123.1 (ArCH), 122.5 (ArCH).

2-Chloropyridinyl-4-methylenediethylphosphonate. 2-Chloronicotinic acid (3.00 g, 19.0 mmol) was dissolved in dry THF (60 mL) and cooled to 0 °C. Lithium aluminium hydride (870 mg, 23.0 mmol) was charged into the stirred reaction (CAUTION: gas evolution) followed by gradual warming to reflux for 4 h. The reaction was quenched with sequential addition of wet THF (5 mL) and water (50 mL, cautiously) before filtration through Celite and removal of volatiles *in vacuo* gave yellow oil that was purified by flash chromatography (SiO_2, CH_2Cl_2 followed by EtOAc). The crystalline alcohol was dissolved in CH_2Cl_2 (20 mL) and excess thionylchloride (5−10 mL) before refluxing for 1 h. On cooling to room temperature, volatiles were removed *in vacuo* and the residue neutralized with sat. $NaHCO_3$ before extraction with CH_2Cl_2 (3 × 40 mL). Organics were combined, dried over $MgSO_4$, filtered, and concentrated to 3−5 mL before purification through a silica plug (eluting with CH_2Cl_2). Removal of volatiles *in vacuo* gave yellow oil as the desired 2-chloropyridyl-5-methylene chloride. The alkyl chloride was dissolved in triethylphosphite (10 mL) and heated to 140 °C for 2 h. On cooling to room temperature, volatiles were removed *in vacuo* and the residue purified by flash chromatography (SiO_2, CH_2Cl_2 followed by EtOAc)

to give a light yellow oil (3.30, 65%). ^{1}H NMR (500 MHz; $CDCl_3$): δ/ppm 8.28−8.26 (m, 1H, Py-*H*), 7.64 (dt, 1H, $^3J_{HH}$ = 8.2, $^4J_{HH}$ = 2.5, Py-*H*), 7.28 (d, 1H, $^3J_{HH}$ = 8.2, Py-*H*), 4.09−4.02 (m, 4H, O−CH_2), 3.09 (d, 2H, $^3J_{HP}$ = 21.6, O═P−CH_2), 1.28−1.25 (m, 6H, CH_3). ^{13}C{^{1}H} NMR (125.7 MHz; $CDCl_3$): δ/ppm 150.4 (d, $^3J_{CP}$ = 7.7, PyCH), 150.3 (d, $^5J_{CP}$ = 4, PyC-Cl), 140.0 (d, $^3J_{CP}$ = 5.5, PyCH), 127.1 (d, $^2J_{CP}$ = 9, PyC), 124.2 (d, $^4J_{CP}$ = 2.9, PyCH), 62.6 (d, $^2J_{CP}$ = 6.8, O-*C*H_2), 30.5 (d, $^1J_{CP}$ = 140.0, O═P-*C*H_2), 16.5 (d, $^3J_{CP}$ = 5.9, CH_2-*C*H_3). ^{31}P{^{1}H} NMR (202.5 MHz; $CDCl_3$): δ/ppm 24.8 (s, O═*P*).

(E)-2-Chloro-pyridinyl-4-(4′-N,N-dimethylaminostilbene). 2-Chloropyridyl-5-methylenediethylphosphonate (2.0 g, 3.60 mmol) and 4-*N,N*-dimethylbenzaldehyde (1.14 g, 3.60 mmol) were dissolved with stirring in dry dimethylformamide (10 mL) at room temperature. Sodium hydride (720 mg, 60%w/w, 8.0 mmol) was charged into the stirred reaction (CAUTION: gas evolution) causing an immediate color change to deep red over the period of 2 h. The reaction was quenched with addition of water (20 mL, cautiously), precipitating the crude product that was filtered and washed repeatedly with water to remove trace dimethylformamide. The crude yellow product was subsequently dissolved in CH_2Cl_2 (50 mL) and washed with water (3 × 10 mL) before organics were separated, dried over $MgSO_4$, filtered, and removed of volatiles *in vacuo* to give a fine yellow solid (1.12 g, 57%). ^{1}H NMR (500 MHz; DMSO-d_6): δ/ppm 8.51 (d, $^4J_{HH}$ = 2.2, 1H, PyH), 8.03 (dd, $^3J_{HH}$ = 8.4, $^4J_{HH}$ = 2.3, 1H, PyH), 7.44 (d, $^4J_{HH}$ = 8.4, 1H, PyH), 7.40 (m, AA′BB′, 2H, ArH), 7.27 (m, AB, 1H, CH═CH), 6.97 (m, AB, 1H, CH═CH), 6.72 (m, AA′BB′, 2H, ArH), 2.94 (s, 6H, N(CH_3)$_2$). ^{13}C{^{1}H} NMR (125.7 MHz; DMSO-d_6): δ/ppm 150.3 (Ar*C*), 147.5 (Py*C*), 147.4 (PyCH), 135.4 (Py*C*H), 133.3 (Py*C*), 131.8 (H*C*═CH), 127.9 (ArCH), 124.2 (Ar*C*), 124.1 (PyCH), 118.2 (H*C*═CH), 112.1 (ArCH), 39.8 (N(*C*H_3)$_2$).

2-Hydrazino-pyridinyl-2-benzothiazole. 2-Chloropyridine-4-benzothiazole (500 mg, 2.23 mmol) and hydrazine hydrate (5 mL) were refluxed in ethanol (30 mL) under nitrogen for 4 h. A light yellow precipitate formed that on cooling to room temperature, was collected, washed with ethanol, diethyl ether, and air-dried (460 mg, 94%). ^{1}H NMR (500 MHz; DMSO-d_6): δ/ppm 8.69 (s, 1H, PyH), 8.28 (s, 1H, NH-Py), 8.09−8.05 (m, 2H, PyH & ArH), 7.94 (d, $^3J_{HH}$ = 7.7, 1H, ArH), 7.48 (t, $^3J_{HH}$ = 7.1, 1H, ArH), 7.36 (m, 1H, ArH), 6.86−6.84 (m, 1H, PyH), 4.39 (s, 2H, N*H*$_2$-NH). ^{13}C{^{1}H} NMR (125.7 MHz; DMSO-d_6): δ/ppm 165.8 (Bz*C*), 163.0 (PyCNH), 153.6 (Ar*C*), 147.4 (Py*C*H), 135.5 (PyCH), 133.5 (Ar*C*), 126.4 (ArCH), 124.6 (ArCH), 122.0 (ArCH), 121.9 (Ar*C*H), 117.8 (Py*C*), 105.8 (PyCH).

(E)-2-Hydrazino-pyridinyl-4-(4′-N,N-dimethylaminostilbene). (*E*)-2-Chloro-pyridinyl-4-(4′-*N,N*-dimethylaminostilbene) (1.0 g, 3.86 mmol) was refluxed in hydrazine hydrate (30 mL) under nitrogen for 16 h. A colorless precipitate formed, that on cooling to room temperature was collected, washed repeatedly with water, followed by diethyl ether, and air-dried (910 mg, 93%). ^{1}H NMR (500 MHz; DMSO-d_6): δ/ppm 8.08 (bs, 1H, PyH), 7.73 (bm, 1H, PyH), 7.49 (bs, 1H, NH-Py), 7.35 (m, AA′BB′, 2H, ArH), 6.85 (aq, AB, 2H, CH═CH), 6.70 (m, AA′BB′, 2H, ArH), 4.15 (s, 2H, N*H*$_2$-NH), 2.91 (s, 6H, N(CH_3)$_2$). ^{13}C{^{1}H} NMR (125.7 MHz; DMSO-d_6): δ/ppm 160.8 (Py*C*), 149.5 (Ar*C*), 146.2 (PyCH), 133.1 (Py*C*H), 126.8 (ArCH), 125.6 (Ar*C*), 124.8 (H*C*═CH), 122.8 (Py*C*), 121.0 (H*C*═CH), 112.3 (ArCH), 106.5 (Py*C*H), 40.0 (N(*C*H_3)$_2$).

*N,N-Dimethylaminoethylisothiocyanate (**4**).*[83] Dicyclohexylcarbodiimide (2.0 g, 8.80 mmol) and CS_2 (600 uL, 8.80 mmol) were dissolved in ether (50 mL) and cooled to 0 °C. *N,N*-Dimethylethylene diamine (1.0 mL, 8.80 mmol) was subsequently added dropwise over 5 min to the cooled solution resulting in precipitation of a colorless solid. The reaction was allowed to warm to room temp over 2 h with monitoring by TLC (ether). The reaction was filtered and the filtrate was concentrated to dryness. The residue was chromatographed (SiO_2, ether) to yield a colorless low melting solid (380 mg, 33%). ^{1}H NMR (400 MHz; DMSO-d_6): δ/ppm 3.71 (t, $^3J_{HH}$ = 6.0, 2H, CH_2), 2.60 (t, $^3J_{HH}$ = 6.0, 2H, CH_2), 2.27 (s, 6H, N(CH_3)$_2$).

*4-N,N-Dimethylaminoethyl-3-thiosemicarbazide (**5**).* *N,N*-Dimethylaminoethylisothiocyanate (380 mg, 2.91 mmol) was dissolved in methanol (25 mL) and treated with hydrazine hydrate (300 μL, 6.00 mmol) at room temp. The reaction was monitored by TLC (ether) and complete after 20 min. Concentration to dryness gave a colorless crystalline solid that was collected and washed with ether (400 mg, 85%). ^{1}H NMR (400 MHz; DMSO-d_6): δ/ppm 8.62 (bs, 1H, N*H*−C═S), 7.78 (bs, 1H, N*H*−C═S), 4.44 (bs, 2H, N−N*H*$_2$), 3.50 (q, $^3J_{HH}$ = 5.9, 2H, CH_2), 2.36 (t, $^3J_{HH}$ = 6.4, 2H, CH_2), 2.15 (s, 6H, N(CH_3)$_2$). MS(ES$^+$) *m*/*z* (calcd) 163.1597 (163.0973) {M + H$^+$}.

*Diacetyl-mono-4-N,N-dimethylaminoethyl-3-thiosemicarbazone (**6**).* 4-*N,N*-Dimethylaminoethyl-3-thiosemicarbazide (400 mg, 2.46 mmol) was dissolved in methanol (25 mL) and subsequently added dropwise over 1 h to a cooled solution of 2,3-butanedione (1.1 mL, 12.3 mmol) in methanol (50 mL) in the presence of catalytic HCl. The reaction was monitored by TLC (CH_2Cl_2) and on completion concentrated to dryness. The residue was extracted with CH_2Cl_2 (3 × 25 mL), washed with sat. sodium bicarbonate solution, before organic fractions were collated, dried over $MgSO_4$, and removed of volatiles. The residue was chromatographed (SiO_2, CH_2Cl_2) to give a yellow crystalline solid (420 mg, 74%). ^{1}H NMR (400 MHz; DMSO-d_6): δ/ppm 10.74 (s, 1H, N−N*H*−C═S), 8.56 (s, 1H, CH_2−N*H*−C═S), 3.61 (q, $^3J_{HH}$ = 5.9, 2H, CH_2), 2.46 (t, $^3J_{HH}$ = 6.5, 2H, CH_2), 2.35 (s, 3H, N═C−CH_3) 2.18 (s, 6H, N(CH_3)$_2$), 1.94 (s, 3H, O═C−CH_3). MS(ES$^+$) *m*/*z* (calcd) 231.2018 (231.1235) {M + H$^+$}.

*Diacetyl-2-(2-hydrazino-pyridinyl-4-benzothiazole)-(4-methyl-3-thiosemicarbazone) (**H_2L^1**).* 2-Hydrazinopyridine-4-benzothiazole (150 mg, 0.62 mmol) and diacetyl-mono-4-methyl-3-thiosemicarbazone (120 mg, 0.62 mmol) were refluxed in ethanol (30 mL) under nitrogen for 4 h in the presence of catalytic acetic acid. A yellow precipitate formed that on cooling to room temperature, was collected, washed with ethanol, then ether, and air-dried (195 mg, 76%). Elem. anal. Found (calcd) for $C_{18}H_{19}N_7S_2$: C, 54.42 (54.39); H, 4.77 (4.82); N, 24.86 (24.66). ^{1}H NMR (500 MHz; DMSO-d_6): δ/ppm 10.49 (s, 1H, N−N*H*−C═S), 10.18 (s, 1H, N−N*H*−C═S), 8.88 (d, $^4J_{HH}$ = 2.4, 1H, PyH), 8.35−8.33 (m, 1H, CH_3−N*H*−C═S), 8.30 (dd, $^3J_{HH}$ = 8.8, $^4J_{HH}$ = 2.4, 1H, PyH), 8.11 (d, $^3J_{HH}$ = 8, 1H, ArH), 8.01 (d, $^3J_{HH}$ = 8, 1H, ArH), 7.52 (td, $^3J_{HH}$ = 8, $^4J_{HH}$ = 1, 1H, ArH), 7.44−7.39 (m, 2H, PyH & ArH), 3.04 (d, $^3J_{HH}$ = 4.6, 3H, NH−CH_3), 2.27 (s, 3H, N═C−CH_3), 2.25 (s, 3H, N═C−CH_3). MS(ES$^+$) *m*/*z* (calcd) 398.1210 (398.1143) {M + H$^+$}. HPLC R_t 14.56 min.

*Diacetyl-2-((E)-2-hydrazino-pyridinyl-4-(4′-N,N-dimethylaminostilbene))-(4-methyl-3-thiosemicarbazone) (**H_2L^2**).* (*E*)-2-Hydrazino-pyridinyl-4-(4′-*N,N*-dimethylaminostilbene) (95 mg, 0.37 mmol) and diacetyl-mono-4-methyl-3-thiosemicarbazone (65 mg, 0.37 mmol) were refluxed in ethanol (30 mL) under nitrogen for 4 h in the presence of catalytic acetic acid. A yellow precipitate formed that, on cooling to room temperature, was collected, washed with ethanol, then ether, and air-dried (130 mg, 85%). Elem. anal. Found (calcd) for $C_{21}H_{27}N_7S$: C, 61.40 (61.59); H, 6.75 (6.64); N, 23.85 (23.94). ^{1}H NMR (500 MHz; DMSO-d_6): δ/ppm 10.12 (s, 1H, N−N*H*−C═S), 9.98 (s, 1H, N−N*H*−Py), 8.31 (m, 1H, CH_3−N*H*−C═S), 8.29 (d, $^4J_{HH}$ = 2.2, 1H, PyH), 7.82 (dd, $^3J_{HH}$ = 8.8, $^4J_{HH}$ = 2.3, 1H, PyH), 7.40 (m, AA′BB′, 2H, ArH), 7.25 (d, $^3J_{HH}$ = 8.7, 1H, PyH), 7.04 (m, AB, 1H, CH═CH), 6.92 (m, AB, 1H, CH═CH), 6.72 (m, AA′BB′, 2H, ArH), 3.04 (d, 3H, $^3J_{HH}$ = 4.6, NH−CH_3), 2.92 (s, 6H, N(CH_3)$_2$), 2.23 (s, 3H, N═C−CH_3), 2.22 (s, 3H, N═C−CH_3). ^{13}C{^{1}H} NMR (125.7 MHz; DMSO-d_6): δ/ppm 183.6 (*C*═S), 160.9 (Py*C*), 155.0 (Ar*C*), 153.9 (*C*═N−N), 151.2 (PyCH), 149.4 (*C*═N−N), 139.5 (PyCH), 132.4 (ArCH), 132.1 (H*C*═CH), 131.4 (Py*C*), 130.5 (Ar*C*), 125.5 (H*C*═CH), 117.5 (Ar*C*H), 112.3 (PyCH), 45.2 (N(*C*H_3)$_2$), 36.3 (NH-CH_3), 16.6 (N═C−CH_3), 16.1 (N═C−CH_3). MS(ES$^+$) *m*/*z* (calcd) 410.1915 (410.2049) {M + H$^+$}. HPLC R_t 11.43 min.

*Diacetyl-2-((E)-2-hydrazino-pyridinyl-4-(4′-N,N-dimethylaminostilbene))-(4-dimethylaminoethyl-3-thiosemicarbazone) (**H_2L^3**).* (*E*)-2-Hydrazino-pyridinyl-4-(4′-*N,N*-dimethylaminostilbene) (100 mg, 0.39 mmol) and diacetyl-mono-4-dimethylaminoethyl-3-thiosemicarbazone (110 mg, 0.47 mmol) were refluxed in ethanol (30 mL) under nitrogen for 4 h in the presence of catalytic conc. HCl. The reaction was followed by TLC (EtOAc), and on completion allowed to cool to room temperature before filtration through Celite. The filtrate was concentrated to 5 mL before trituration with diethyl ether precipitated a crystalline yellow solid. The precipitate was collected, washed with

dx.doi.org/10.1021/ja4057807 | J. Am. Chem. Soc. 2013, 135, 16120−16132

ether, and air-dried (80 mg, 44%). Elem. anal. Found (calcd) for $C_{24}H_{37}Cl_3N_8S$: C, 50.40 (50.04); H, 7.00 (6.47); N, 19.30 (19.45). ^{1}H NMR (500 MHz; DMSO-d_6): δ/ppm 10.47 (s, 1H, N−N*H*−C═S), 10.04 (s, 1H, N−N*H*−Py), 9.95 (bs, 1H, [C−N*H*$(CH_3)_2$]$^+$), 8.47 (m, 1H, CH_2−N*H*−C═S), 8.28 (d, $^4J_{HH}$ = 2.2, 1H, PyH), 7.90 (m, 1H, PyH), 7.38 (m, AA′BB′, 2H, ArH), 7.24 (d, $^3J_{HH}$ = 8.8, 1H, PyH), 7.03 (m, AB, 1H, CH═CH), 6.91 (m, AB, 1H, CH═CH), 6.70 (m, AA′BB′, 2H, ArH), 3.95 (m, 2H, N−CH_2), 2.91 (s, 6H, Ar−N$(CH_3)_2$), 2.81 (bs, 6H, N$(CH_3)_2$), 2.24 (s, 3H, N═C−CH_3), 2.22 (s, 3H, N═C−CH_3). ^{13}C{^{1}H} NMR (125.7 MHz; DMSO-d_6): δ/ppm 178.1 (*C*═S), 155.6 (PyC), 149.8 (ArC), 149.8 (*C*═N−N), 146.0 (PyCH), 144.0 (*C*═N−N), 134.3 (PyCH), 127.2 (ArCH), 126.9 (HC═CH), 126.3 (PyC), 125.2 (ArC), 120.3 (HC═CH), 112.3 (ArCH), 107.2 (PyCH), 55.2 (CH_2N$(CH_3)_2$), 42.7 (N$(CH_3)_2$), 40.0 (Ar−N$(CH_3)_2$), 38.9 (N−CH_2), 11.7 (N═C−CH_3), 11.0 (N═C−CH_3). MS(ES$^+$) *m*/*z* (calcd) 467.2693 (467.2627) {M + H$^+$}. HPLC R_t 9.24 min.

*Diacetyl-2-(2-hydrazino-pyridinyl-4-benzothiazole)-(4-methyl-3-thiosemicarbazonato) copper(II) (Cu^{II}**L**^{1}).* H_2**L**^{1} (50 mg, 0.12 mmol) and copper(II) acetate monohydrate (27 mg, 0.13 mmol) were refluxed in ethanol (10 mL) under nitrogen for 2 h. A dark purple precipitate formed that, on cooling to room temperature, was collected, washed with ethanol (3 × 5 mL), and air-dried (15 mg, 27%). Elem. anal. Found (calcd) for $C_{18}H_{17}CuN_7S_2$: C, 46.75 (47.10); H, 3.66 (3.73); N, 21.64 (21.36). MS(ES$^+$) *m*/*z* (calcd) 459.0166 (459.0283) {M + H$^+$}. HPLC R_t 13.49 min. Crystals suitable for single-crystal X-ray diffraction were grown from slow diffusion of diethyl ether at room temperature into a degassed solution of H_2**L**^{1} and [Cu$(CH_3CN)_4$]BF_4 in dimethylformamide.

*Diacetyl-2-((E)-2-hydrazino-pyridinyl-4-(4′-N,N-dimethylaminostilbene))-(4-methyl-3-thiosemicarbazonato) Copper(II) (Cu^{II}**L**^{2}).* H_2**L**^{2} (115 mg, 0.28 mmol) was dissolved in dichloromethane (30 mL) heated to reflux and subsequently treated with copper(II) acetate (67 mg, 0.32 mmol). The reaction darkened immediately affording a deep blue solution that was stirred for 2 h. On cooling to room temperature the reaction was filtered through Celite and concentrated by half precipitating a near black solid that was collected, washed with diethyl ether, and air-dried (122 mg, 92%). Elem. anal. Found (calcd) for $C_{21}H_{25}CuN_7S$: C, 53.47 (53.54); H, 4.96 (5.35); N, 20.64 (20.81). MS(ES$^+$) *m*/*z* (calcd) 471.1264 (471.1188) {M + H$^+$}. HPLC R_t 11.79 min. Crystals suitable for single-crystal X-ray diffraction were obtained from the air oxidation of Cu^I complex [Cu$^I_2$(H_2**L**^{2})$_2$]$(BF_4)_2$, the preparation of which is outlined below.

*[Cu$^I_2$(H_2**L**^{2})$_2$]$(BF_4)_2$.* H_2**L**^{2} (20 mg, 0.05 mmol) and [Cu$(CH_3CN)_4$]-BF_4 (16 mg, 0.05 mmol) were charged into a pencil Schlenk tube and dissolved in degassed dimethylformamide (5 mL). After standing for 30 min at room temperature the sample was frozen and in liquid N_2 prior to the slow addition of degassed diethyl ether. Red crystals of [Cu$^I_2$(H_2**L**^{2})$_2$]$(BF_4)_2$ suitable for single-crystal X-ray diffraction grew from slow diffusion of diethyl ether at room temperature into the concentrated dimethylformamide complex solution. Crystallographic details are given in Table 1.

*Diacetyl-2-((E)-2-hydrazino-pyridinyl-4-(4′-N,N-dimethylaminostilbene))-(4-dimethylaminoethyl-3-thiosemicarbazonato) Copper-(II) (Cu^{II}**L**^{3}).* H_2**L**^{3} (20 mg, 0.04 mmol) was suspended in dichloromethane (10 mL) and heated to near reflux. Copper(II) acetate (10 mg, 0.05 mmol) was added to the reaction causing a gradual solution color change to near black. The reaction was refluxed for 2 h with monitoring by TLC (10%MeOH/DCM/0.1%NEt_3). The reaction was removed from heat and concentrated to dryness. The residue was purified by flash chromatography eluting deep blue fractions (12 mg, 54%). MS(ES$^+$) *m*/*z* (calcd) 528.1841 (528.1767) {M + H$^+$}. HPLC R_t 9.35 min.

■ ASSOCIATED CONTENT

Ⓢ Supporting Information

The electronic spectroscopy for Cu**L**$^{1-3}$, data used for the generation of the apparent conditional dissociation constant of Cu^{II}**L**^{3}, and figures showing the treatment of AD brain sections with metal-free ligand H_2**L**^{3}. This material is available free of charge via the Internet at http://pubs.acs.org.

■ AUTHOR INFORMATION

Corresponding Author

*E-mail: pauld@unimelb.edu.au.

Notes

The authors declare no competing financial interest.

■ ACKNOWLEDGMENTS

Financial support from the Australian Research Council and the National Health and Medical Research Council (Australia). The Victorian Brain Bank Network for the provision of human tissue. Clarity Pharmaceuticals for the provision of $^{64}CuCl_2$. Kerry Ardley and Susan Jackson for their technical expertise in performing the PET scanning and mouse biodistribution. Prof Rodney Hicks (Peter MacCallum Cancer Centre) for assistance in the interpretation of the small animal imaging.

■ REFERENCES

(1) Karran, E.; Mercken, M.; De Strooper, B. *Nat. Rev. Drug Discovery* **2011**, *10*, 698.

(2) Masters, C. L.; Simms, G.; Weinman, N. A.; Multhaup, G.; McDonald, B. L.; Beyreuther, K. *Proc. Natl. Acad. Sci. (USA)* **1985**, *82*, 4245.

(3) Hardy, J. A.; Higgins, G. A. *Science* **1992**, *256*, 184.

(4) Kung, H. F.; Choi, S. R.; Qu, W.; Zhang, W.; Skovronsky, D. *J. Med. Chem.* **2010**, *53*, 933.

(5) Rowe, C. C.; Villemagne, V. L. *J. Nucl. Med.* **2011**, *52*, 1733.

(6) Chen, X. *THEOCHEM* **2006**, *763*, 83.

(7) Klunk, W. E.; Wang, Y.; Huang, G.-F.; Debnath, M. L.; Holt, D. P.; Mathis, C. A. *Life Sci.* **2001**, *69*, 1471.

(8) Mathis, C. A.; Bacskai, B. J.; Kajdasz, S. T.; McLellan, M. E.; Frosch, M. P.; Hyman, B. T.; Holt, D. P.; Wang, Y.; Huang, G.-F.; Debnath, M. L.; Klunk, W. E. *Bioorg. Med. Chem. Lett.* **2002**, *12*, 295.

(9) Kung, H. F.; Lee, C.-W.; Zhuang, Z.-P.; Kung, M.-P.; Hou, C.; Ploessl, K. *J. Am. Chem. Soc.* **2001**, *123*, 12740.

(10) Mathis, C. A.; Wang, Y.; Holt, D. P.; Huang, G.-F.; Debnath, M. L.; Klunk, W. E. *J. Med. Chem.* **2003**, *46*, 2740.

(11) Lopresti, B. J.; Klunk, W. E.; Mathis, C. A.; Hoge, J. A.; Ziolko, S. K.; Lu, X.; Meltzer, C. C.; Schimmel, K.; Tsopelas, N. D.; DeKosky, S. T.; Price, J. C. *J. Nucl. Med.* **2005**, *46*, 1959.

(12) Villemagne, V. L.; Pike, K. E.; Chetelat, G.; Ellis, K. A.; Mulligan, R. S.; Bourgeat, P.; Ackermann, U.; Jones, G.; Szoeke, C.; Salvado, O.; Martins, R.; O'Keefe, G.; Mathis, C. A.; Klunk, W. E.; Ames, D.; Masters, C. L.; Rowe, C. C. *Ann. Neurol.* **2010**, *69*, 181.

(13) Ono, M.; Wilson, A.; Nobrega, J.; Westaway, D.; Verhoeff, P.; Zhuang, Z.-P.; Kung, M.-P.; Kung, H. F. *Nucl. Med. Biol.* **2003**, *30*, 565.

(14) Verhoeff, N. P. L. G.; Wilson, A., A.; Takeshita, S.; Trop, L.; Hussey, D.; Singh, K.; Kung, H., F.; Kung, M.-P.; Houle, S. *Am. J. Geriat. Psychiat.* **2004**, *12*, 584.

(15) Rowe, C.; Ackerman, U.; Browne, W.; Mulligan, R.; Pike, K. L.; O'Keefe, G.; Tochon-Danguay, H.; Chan, G.; Berlangieri, S. U.; Jones, G.; Dickinson-Rowe, K. L.; Kung, H. P.; Zhang, W.; Kung, M. P.; Skovronsky, D.; Dyrks, T.; Hall, G.; Krause, S.; Friebe, M.; Lehman, L.; Lindemann, S.; Dinkelborg, L. M.; Masters, C. L.; Villemagne, V. L. *Lancet Neurol.* **2008**, *7*, 129.

(16) Zhang, W.; Oya, S.; Kung, M.-P.; Hou, C.; Maier, D. L.; Kung, H. F. *J. Med. Chem.* **2005**, *48*, 5980.

(17) Qu, W.; Kung, M.-P.; Hou, C.; Benedum, T. E.; Kung, H. F. *J. Med. Chem.* **2007**, *50*, 2157.

(18) Zhang, W.; Kung, M.-P.; Oya, S.; Hou, C.; Kung, H. F. *Nucl. Med. Biol.* **2007**, *34*, 89.

(19) Choi, S. R.; Golding, G.; Zhuang, Z.; Zhang, W.; Lim, N.; Hefti, F.; Benedum, T. E.; Kilbourn, M. R.; Skovronsky, D.; Kung, H. F. *J. Nucl. Med.* **2009**, *50*, 1887.

(20) Yang, L.; Rieves, D.; Ganley, C. *New Engl. J. Med.* **2012**, *367*, 885.
(21) Clark, C. M.; Pontecorvo, M. J.; Beach, T. G.; Bedell, B. J.; Coleman, R. E.; Doraiswamy, P. M.; Fleisher, A. S.; Reiman, E. M.; Sabbagh, M. N.; Sadowsky, C. H.; Schneider, J. A.; Arora, A.; Carpenter, A. P.; Flitter, M. L.; Joshi, A. D.; Krautkramer, M. J.; Lu, M.; Mintun, M. A.; Skovronsky, D. M. *Lancet Neurol.* **2012**, *11*, 669.
(22) Blower, P. J.; Lewis, J. S.; Zweit, J. *Nucl. Med. Biol* **1996**, *23*, 957.
(23) Smith, S. V. *J. Inorg. Biochem.* **2004**, *98*, 1874.
(24) Wadas, T. J.; Wong, E. H.; Weisman, G. R.; Anderson, C. J. *Chem. Rev.* **2010**, *110*, 2858.
(25) Donnelly, P. S. *Dalton Trans.* **2011**, *40*, 999.
(26) Hickey, J. L.; Donnelly, P. S. *Coord. Chem. Rev.* **2012**, *256*, 2367.
(27) Fujibayashi, Y.; Taniuchi, H.; Yonekura, Y.; Ohtani, H.; Konishi, J.; Yokoyama, A. *J. Nucl. Med.* **1997**, *38*, 1155.
(28) Vavere, A. L.; Lewis, J. S. *Dalton Trans.* **2007**, 4893.
(29) Lim, S.; Paterson, B. M.; Fodero-Tavoletti, M. T.; O'Keefe, G. J.; Cappai, R.; Barnham, K. J.; Villemagne, V. L.; Donnelly, P. S. *Chem. Commun.* **2010**, *46*, 5437.
(30) Holland, J. P.; Aigbirhio, F. I.; Betts, H. M.; Bonnitcha, P. D.; Burke, P.; Christlieb, M.; Churchill, G. C.; Cowley, A. R.; Dilworth, J. R.; Donnelly, P. S.; Green, J. C.; Peach, J. M.; Vasudevan, S. R.; Warren, J. E. *Inorg. Chem.* **2007**, *46*, 465.
(31) Cowley, A. R.; Dilworth, J. R.; Donnelly, P. S.; White, J. M. *Inorg. Chem.* **2006**, *45*, 496.
(32) Cowley, A. R.; Dilworth, J. R.; Donnelly, P. S.; Labisbal, E.; Sousa, A. *J. Am. Chem. Soc.* **2002**, *124*, 5270.
(33) Alsop, L.; Cowley, A. R.; Dilworth, J. R.; Donnelly, P. S.; Peach, J. M.; Rider, J. T. *Inorg. Chim. Acta* **2005**, *358*, 2770.
(34) Barnard, P. J.; Bayly, S. R.; Holland, J. P.; Dilworth, J. R.; Waghorn, P. A. *Q. J. Nucl. Med. Mol. Imaging* **2008**, *52*, 235.
(35) Dickens, M. G.; Franz, K. J. *ChemBioChem* **2010**, *11*, 59.
(36) Perez, L. R.; Franz, K. J. *Dalton Trans.* **2010**, *39*, 2177.
(37) Leed, M. G. D.; Wolkow, N.; Pham, D. M.; Daniel, C. L.; Dunaief, J. L.; Franz, K. J. *J. Inorg. Biochem.* **2011**, *105*, 1161.
(38) Hyman, L. M.; Franz, K. J. *Coord. Chem. Rev.* **2012**, *256*, 2333.
(39) Kielar, F.; Helsel, M. E.; Wang, Q.; Franz, K. J. *Metallomics* **2012**, *4*, 899.
(40) Xiao, Z..; Wedd, A. G. *Nat. Prod. Rep.* **2010**, *27*, 768.
(41) Telpoukhovskaia, M. A.; Orvig, C. *Chem. Soc. Rev.* **2013**, *42*, 1836.
(42) Zawisza, I.; Rozga, M.; Bal, W. *Coord. Chem. Rev.* **2012**, *256*, 2297.
(43) Alies, B.; Renaglia, E.; Rozga, M.; Bal, W.; Faller, P.; Hureau, C. *Anal. Chem.* **2013**, *85*, 1501.
(44) Drew, S. C.; Barnham, K. J. *Acc. Chem. Res.* **2011**, *44*, 1146.
(45) Hureau, C. *Coord. Chem. Rev.* **2012**, *256*, 2164.
(46) Fodero-Tavoletti, M. T.; Smith, D. P.; McLean, C. A.; Adlard, P. A.; Barnham, K. J.; Foster, L. E.; Leone, L.; Perez, K.; Cortes, M.; Culvenor, J. G.; Li, Q.-X.; Laughton, K. M.; Rowe, C. C.; Masters, C. L.; Cappai, R.; Villemagne, V. L. *J. Neurosci.* **2007**, *27*, 10365.
(47) Smith, S. V.; Jones, M.; Holmes, V., Eds. In *Production and Selection of Metal PET Radioisotopes for Molecular Imaging*; InTech, 2011; Vol *10*.
(48) Petering, D. H. *Biochem. Pharmacol.* **1974**, *23*, 567.
(49) Green, M. A.; Klippenstein, D. L.; Tennison, J. R. *J. Nucl. Med.* **1988**, *29*, 1549.
(50) Price, K. A.; Crouch, P. J.; Volitakis, I.; Paterson, B. M.; Lim, S.; Donnelly, P. S.; White, A. R. *Inorg. Chem.* **2011**, *50*, 9594.
(51) Paterson, B. M.; Donnelly, P. S. *Chem. Soc. Rev.* **2011**, *40*, 3005.
(52) Fodero-Tavoletti, M. T.; Villemagne, V. L.; Paterson, B. M.; White, A. R.; Li, Q.-X.; Camakaris, J.; O'Keefe, G.; Cappai, R.; Barnham, K. J.; Donnelly, P. S. *J. Alz. Dis.* **2010**, *20*, 49.
(53) Dearling, J. L. J.; Lewis, J. S.; McCarthy, D. W.; Welch, M. J.; Blower, P. J. *J. Chem. Soc., Chem. Commun.* **1998**, 2531.
(54) Green, M. A.; Mathias, C. J.; Welch, M. J.; McGuire, A. H.; Perry, D.; Fernandez-Rubio, F.; Perlmutter, J. S.; Raichle, M. E.; Bergmann, S. R. *J. Nucl. Med.* **1990**, *31*, 1989.
(55) John, E. K.; Green, M. A. *J. Med. Chem.* **1990**, *33*, 1764.
(56) Lewis, J. S.; McCarthy, D. W.; McCarthy, T. J.; Fujibayashi, Y.; Welch, M. J. *J. Nucl. Med.* **1999**, *40*, 177.
(57) Ikawa, M.; Okazawa, H.; Kudo, T.; Kuriyama, M.; Fujibayashi, Y.; Yoneda, M. *Nucl. Med. Biol.* **2011**, *38*, 945.
(58) Ikawa, M.; Okazawa, H.; Arakawa, K.; Kudo, T.; Kimura, H.; Fujibayashi, Y.; Kuriyama, M.; Yoneda, M. *Mitochondrion* **2009**, *9*, 144.
(59) Yates, C. M.; Butterworth, J.; Tennant, M. C.; Gordon, A. *J. Neurochem.* **1990**, *55*, 1624.
(60) Atwood, C. S.; Moir, R. D.; Huang, X.; Scarpa, R. C.; Bacarra, N. M. E.; Romano, D. M.; Hartshorn, M. A.; Tanzi, R. E.; Bush, A. I. *J. Biol. Chem.* **1998**, *273*, 12817.
(61) Dearling, J. L. J.; Lewis, J. S.; Mullen, G. E. D.; Rae, M. T.; Zweit, J.; Blower, P. J. *Eur. J. Nucl. Med.* **1998**, *25*, 788.
(62) Dearling, J. L. J.; Lewis, J. S.; Mullen, G. D.; Welch, M. J.; Blower, P. J. *J. Biol. Inorg. Chem.* **2002**, *7*, 249.
(63) Holland, J. P.; Green, J. C.; Dilworth, J. R. *Dalton Trans.* **2006**, 783.
(64) Dickson, T. C.; Vickers, J. C. *Neuroscience* **2001**, *105*, 99.
(65) Cherny, R. A.; Atwood, C. S.; Xilinas, M. E.; Gray, D. N.; Jones, W. D.; McLean, C. A.; Barnham, K. J.; Volitakis, I.; Fraser, F. W.; Kim, Y.-S.; Huang, X.; Goldstein, L. E.; Moir, R. D.; Lim, J. T.; Beyreuther, K.; Zheng, H.; Tanzi, R. E.; Masters, C. L.; Bush, A. I. *Neuron* **2001**, *30*, 665.
(66) Adlard, P. A.; Cherny, R. A.; Finkelstein, D. I.; Gautier, E.; Robb, E.; Cortes, M.; Volitakis, I.; Liu, X.; Smith, J. P.; Perez, K.; Laughton, K.; Li, Q. X.; Charman, S. A.; Nicolazzo, J. A.; Wilkins, S.; Deleva, K.; Lynch, T.; Kok, G.; Ritchie, C. W.; Tanzi, R. E.; Cappai, R.; Masters, C. L.; Barnham, K. J.; Bush, A. I. *Neuron* **2008**, *59*, 43.
(67) Crouch, P. J.; Savva, M. S.; Hung, L. W.; Donnelly, P. S.; Mot, A. I.; Parker, S. J.; Greenough, M. A.; Volitakis, I.; Adlard, P. A.; Cherny, R. A.; Masters, C. L.; Bush, A. I.; Barnham, K. J.; White, A. R. *J. Neurochem.* **2011**, *119*, 220.
(68) Schugar, H.; Green, D. E.; Bowen, M. L.; Scott, L. E.; Storr, T.; Bohmerle, K.; Thomas, F.; Allen, D. D.; Lockman, P. R.; Merkel, M.; Thompson, K. H.; Orvig, C. *Angew. Chem, Int. Ed.* **2007**, *46*, 1716.
(69) Storr, T.; Merkel, M.; Song-Zhao, G. X.; Scott, L. E.; Green, D. E.; Bowen, M. L.; Thompson, K. H.; Patrick, B. O.; Schugar, H. J.; Orvig, C. *J. Am. Chem. Soc.* **2007**, *129*, 7453.
(70) Hindo, S. S.; Mancino, A. M.; Braymer, J. J.; Liu, Y. H.; Vivekanandan, S.; Ramamoorthy, A.; Lim, M. H. *J. Am. Chem. Soc.* **2009**, *131*, 16663.
(71) Choi, J. S.; Braymer, J. J.; Nanga, R. P. R.; Ramamoorthy, A.; Lim, M. H. *Proc. Natl. Acad. Sci. U.S.A.* **2010**, *107*, 21990.
(72) Braymer, J. J.; Choi, J. S.; DeToma, A. S.; Wang, C.; Nam, K.; Kampf, J. W.; Ramamoorthy, A.; Lim, M. H. *Inorg. Chem.* **2011**, *50*, 10724.
(73) Sharma, A. K.; Pavlova, S. T.; Kim, J.; Finkelstein, D.; Hawco, N. J.; Rath, N. P.; Kim, J.; Mirica, L. M. *J. Am. Chem. Soc.* **2012**, *134*, 6625.
(74) Ritchie, C. W.; Bush, A. I.; Mackinnon, A.; Macfarlane, S.; Mastwyk, M.; MacGregor, L.; Kiers, L.; Cherny, R.; Li, Q.-X.; Tammer, A.; Carrington, D.; Mavros, C.; Volitakis, I.; Xilinas, M.; Ames, D.; Davis, S.; Beyreuther, K.; Tanzi, R. E.; Masters, C. L. *Arch. Neurol.* **2003**, *60*, 1685.
(75) Lannfelt, L.; Blennow, K.; Zetterberg, H.; Batsman, S.; Ames, D.; Harrison, J.; Maters, C. L.; Targum, S.; Bush, A. I.; Murdoch, R.; Wilson, J.; Ritchie, C. W. *Lancet Neurol.* **2008**, *7*, 779.
(76) Waterhouse, R. N. *Mol. Imaging Biol.* **2003**, *5*, 376.
(77) Vasdev, N.; Cao, P.; van Oosten, E. M.; Wilson, A. A.; Houle, S.; Hao, G.; Sun, X.; Slavine, N.; Alhasan, M.; Antich, P. P.; Bonte, F. J.; Kulkarni, P. *MedChemComm* **2012**, *3*, 1228.
(78) Liu, J.; Hajibeigi, A.; Ren, G.; Lin, M.; Siyambalapitiyage, W.; Liu, Z.; Simpson, E.; Parkey, R. W.; Sun, X.; Oz, O. K. *J. Nucl. Med.* **2009**, *50*, 1332.
(79) Mendes, F.; Paulo, A.; Santos, I. *Dalton Trans.* **2011**, *40*, 5377.
(80) Kuhn, B.; Mohr, P.; Stahl, M. *J. Med. Chem.* **2010**, *53*, 2601.
(81) Jeffery, C. M.; Smith, S. V.; Asada, A. H.; Chana, S.; Price, R. I. *AIP Conf. Proc.* **2012**, *1509*, 84.

(82) Dorow, D. S.; Cullinane, C.; Conus, N.; Roselt, P.; Binns, D.; McCarthy, T. J.; McArthur, G. A.; Hicks, R. J. *Eur. J. Nucl. Med. Mol. Imaging* **2006**, *33*, 441.
(83) Henichart, J. P.; Bernier, J. L.; Houssin, R. *Synthesis* **1980**, 311.